ARTICLES

Factors Affecting *d*-Block Metal−Ligand Bond Lengths: Toward an Automated Library of Molecular Geometry for Metal Complexes

Stephanie E. Harris,[†] A. Guy Orpen,*[,†] Ian J. Bruno,[‡] and Robin Taylor[‡]

School of Chemistry, University of Bristol, Bristol BS8 1TS, U.K., and
Cambridge Crystallographic Data Centre, 12 Union Road, Cambridge CB2 1EZ, U.K.

Received March 4, 2005

Metal−ligand (M−L) bond lengths for a range of ligands (carboxylates, chlorides, pyridines, water, tertiary phosphines, and alkenes) and a variety of metals have been retrieved from the Cambridge Structural Database, CSD. Analysis of the factors which affect M−L bond lengths (for example, ligand coordination mode, oxidation state, metal coordination number and geometry, spin and Jahn−Teller effects, and ligand trans to M−L bond) shows that it is generally possible to subdivide the M−L data sets systematically to obtain better defined, unimodal, bond length distributions with means and sample standard deviations (SSDs) which reflect the nature of the bond in question. Typically, the SSDs for the M−L data sets can be reduced to 0.04−0.05 Å by these methods. This work is an extension to tables of bond lengths in organometallic compounds and coordination complexes published in 1989. The importance of the factors which affect M−L bond lengths for particular metal−ligand groups are discussed. From the case studies reported, an algorithm is proposed by which compilation of a library of molecular geometry for metal complexes may be automated. The points that need to be considered to produce such a molecular library from the data stored in the CSD are discussed. The development of such a library would allow users to retrieve chemically well-defined geometric data rapidly and accurately. This should be of use, for example, to crystallographers and molecular modelers.

INTRODUCTION

It is over 15 years since a major collection of bond length statistics and data based on X-ray and neutron crystallography of organometallic and coordination complexes was published in *J. Chem Soc., Dalton Trans.*[1a] These 1989 tables, which gave comprehensive statistics (mean, median etc.) for metal−ligand and intraligand bond lengths and related data, were heavily cited (as was the organic counterpart publication[1b]) and are still a valuable reference today. The tables were compiled from the Cambridge Structural Database (CSD),[2] and metal−ligand distances were grouped according to the ligand type and divided on ligand bonding mode and, in some cases, oxidation state and metal coordination number when there were a reasonable number of structures. This work used a version of the CSD containing 49 854 structures, in which about a fifth (10 000) were metal containing structures of a quality suitable for use in the analysis. Currently, the CSD contains over 300 000 structures, of which about a third (>100 000) contain at least one transition metal and are of a quality suitable for detailed analysis. Therefore, it should now be possible to analyze metal−ligand bond lengths in much greater detail than was feasible for the 1989 table, as predicted by its authors when they stated that 'in the longer term as more structures are determined it will become possible to derive more precise averages by further subdivision of the distributions'.

In light of the approximately 10-fold increase in the number of metal-containing structures, it would be extremely time-consuming to produce a new version of the original bond length tables by the techniques used in the 1989 study. An alternative would be the development of software that allows rapid retrieval of bond length and other statistics on the geometry of chemically well-defined metal−ligand bonds. This would be based on a structural knowledge base or library of intramolecular geometry for coordination and organometallic compounds, which would be compiled from the CSD employing an automated, algorithmic approach. The algorithms and commissioning of the organic version of this library (Mogul) have been reported recently.[3] However, it was recognized in that work that the methods used would not produce satisfactory estimates of metal−ligand bond geometries. This paper reports progress toward the development of an algorithm for the creation of a metallo-organic molecular geometry library.

Such a library would provide easily accessible information for use in model building, refinement restraints, and structure validation and in providing comparative values for crystallographers, molecular modelers, and other chemical scientists. For example, Harding has shown how geometric data, particularly metal−ligand bond lengths from the CSD, could be used in the validation of metalloprotein crystal structures and to provide refinement restraints.[4−6] From the comparison between protein structure and CSD data of Ca, Mg, Mn, Fe, Cu(II), and Zn metals bonded to various donor groups, Harding argues that, except for the highest resolution protein structure determinations, the precision of bond lengths and

* Corresponding author phone: +44 117 928 8158; fax: +44 117 925 1295; e-mail: guy.orpen@bristol.ac.uk.
[†] University of Bristol.
[‡] Cambridge Crystallographic Data Centre.

10.1021/ci0500785 CCC: $30.25
Published on Web 09/21/2005

angles determined in proteins is "not as good" as the precision with which they can be predicted using CSD structural data.[6a] See and co-workers have investigated the influence of coordination number, oxidation state, and specific ligands on M−L bond distances for first-row transition metals.[7] Their study showed that M−L bond lengths typically increase as the metal coordination number increases in order that a metal center obtains a specific bond order sum which is a function of oxidation state and ligands coordinating to the metal. Hocking and Hambley analyzed metal−ligand and intraligand bond lengths to track variation in covalency and ionic bonding effects across the periodic table.[8]

The present work lays the foundation for our planned development of a structural knowledge base for organometallic and coordination complexes. Specifically, we identify the factors which influence metal−ligand bond lengths and evaluate their relative magnitudes and importance. In so doing, we seek to identify the key features of an algorithm that may be used to automatically subdivide sets of metal−ligand bond lengths (and, by implication, other aspects of geometry) categorized in a well-defined manner. Among the criteria that we consider in this paper are the following:

1. The coordination mode of the ligand
2. Whether the metal atom is part of a metal cluster or cage structure
3. Metal oxidation state
4. Metal coordination number
5. Metal coordination geometry
6. Spin state
7. Jahn−Teller effect
8. The trans ligand.

We also consider fundamental questions relating to how one might gain useful information on metal−ligand geometries in cases where the current data in the CSD is sparse or nonexistent.

In this paper, we first report case studies in which bond length data for a series of metal−ligand fragments were subdivided in order to produce unimodal distributions which are chemically well-defined and have reasonably small sample standard deviations (SSDs). Martín and Orpen[9] analyzed metal complexes using data from the CSD to quantify the crystal packing effects on molecular structure. They assumed that eq 1 could be used to partition the variance, σ^2, in bond lengths (or angles, etc.) between intramolecular environmental effects (σ^2_c), "packing" effects due to the crystal environment of a bond (σ^2_p), and the contributions from experimental uncertainties (σ^2_e).

$$\sigma^2 = \sigma^2_c + \sigma^2_p + \sigma^2_e \quad (1)$$

They showed that there appears to be a minimum uncertainty in metal−ligand bond lengths of ca. 0.01 Å, which can be larger for more easily deformed bonds and is due to experimental and, more significantly, packing effects. A detailed study by Orpen and Quayle[10] of metal containing ions came to similar conclusions. In this latter case M−Cl bond length SSDs typically fell in the range of 0.01−0.02 Å for well-behaved species, but much larger SSDs (0.08 Å and greater) were observed for M−Cl distances in more easily deformed species such as $[BiCl_6]^{3-}$. Therefore, in the present study, metal−ligand bond length SSDs in the range of 0.01−0.02 Å would be the best we can realistically expect, and in many cases SSDs of 0.02−0.04 Å might be deemed reasonable.

Table 1. M−L Fragments Studied

ligand, L	metal, M	ligand bonding modes
carboxylate, O_2CC	Co, Rh, Pt	monodentate, chelating, bridging
chloride, Cl	Fe, Hg, Mn, Pd	terminal
water, OH_2	Cu	terminal
pyridine, py	Fe	terminal
tertiary phosphines	Ni, Mo, Re	monodentate
alkene, C(HC)═C(HC)	Rh	η^2

We report below case studies of the division of M−L bond lengths, according to the criteria above, for carboxylate, chlorine, water, pyridine, phosphine, and alkene ligands with a variety of metals, as listed in Table 1. Subsequently, we consider how the lessons learned might be used in the design of a robust algorithm for automated generation of a molecular geometry library for metal complexes. Although the present study is confined to bond lengths, one can safely assume that the approaches described can be extended to other aspects of molecular geometry such as bond and torsion angles, as in the "organic" version of Mogul.[3]

METHODS AND PROCEDURES

Crystal structures containing the molecular fragments in Table 1 were retrieved from the CSD using the OXQUEST program.[11] Only structures which fulfilled all the following criteria were used for the analysis:

1. Coordinates recorded for the entry.
2. R-factor < 0.075.
3. No disorder present in the structure.
4. No errors found in the entry.
5. For multiple determinations of the same structure, only the 'best' structure as determined by the R-factor was retained.

Structures determined by neutron diffraction were not treated differently in this work. We note that there may be advantages in so doing given that neutron data can yield more accurate geometric information than X-ray (if not always as precise).

Standardization of Metal Connectivity. The connectivity description of structures in the CSD is usually defined by the authors' report. For some metals, in particular those in group 12 and Cu and Ag (plus also groups 1, 2, 14, 15, and Tl), those contacts considered as M−L bonds can be inconsistent in the CSD due to the high variability of these distances. Therefore, standardizing the M−L connectivity for these metals is desirable and may be implemented using the MECALC procedure (the basis of which is described in ref 11). MECALC recalculates the metal coordination sphere for a given metal atom based on user-defined limits for M−L distances. This is applied to all structures in the CSD containing the specified metal.

In the present work, MECALC was used to standardize metal connectivity in the study of Hg−Cl and Cu−OH_2 bond lengths (see Table 1). For all the other metals studied, the metal connectivity is consistent throughout the CSD, and so MECALC was not applied. For the Cu−OH_2 search, all Cu−O and Cu−halogen bonds were included that were of length less than the sum of the covalent radii + 0.6 Å (using CSD standard values).[2] Inspection of histograms of Cu−O/halogen bond lengths showed that increasing the distances

any further gave only a few extra hits and began to include unwanted examples. The connectivity was not recalculated for nitrogen and other ligands in the present study as the Cu connectivity was reasonably consistent for these ligands.

For the Hg−Cl study, Hg−Cl bonds were included that were of length less than the sum of the CSD covalent radii for Hg and Cl + 0.5 Å. It has been argued that a Hg−Cl distance up to 3.35 Å is to be preferred.[12] However inspection of Hg−Cl histograms shows that increasing the Hg−Cl bonded distance to 3.35 Å leads to inclusion of numerous asymmetrically bridging or triply bridging Cl ligands. Alternatively, long Hg−Cl "bonds" (>3.1 Å) have been described[13] as Hg−Cl intermolecular contacts which form supramolecular networks. Therefore, 3.19 Å seems a reasonable cutoff distance for our analysis with the *proviso* that an alternative Hg−Cl bond limit might be advisable in future work. Finally, for the Hg−Cl data set there was no recalculation of other Hg−L bonds, as the CSD entries were consistent.

Metal Clusters/Cages. Metal−metal bonds are not assigned consistently in the CSD. Therefore, the MECALC procedure should ideally be used on all metal clusters to standardize the M−M connectivity. However, in the examples studied here (Table 1) the number of metal cluster structures (i.e. those with multiple M−M bonds) were generally small and could be assigned by hand. All M−M distances less than 3.1 Å were considered to be M−M bonds. In addition, Re−M distances < 3.3 Å and Pd−M and Cu−M < 3.2 Å were defined to be M−M bonds. In this way all formal (on electron counting grounds) M−M bonds were included. An M−L fragment was then defined as being part of a metal cluster if the metal atom in question was bonded to at least two other metal atoms. Standardized metal−metal connectivity is also important for consistent assignment of metal coordination number (see below). For a few structures (mainly for bridging carboxylate fragments) the calculated coordination number needed to be altered to take account of M−M bonds (<3.1 Å) not assigned in the CSD.

Oxidation State. The oxidation state of individual atoms is not reliably searchable in standard CSD software (the Conquest or QUEST3D programs). However, the program OXQUEST has been developed by Shields et al. to calculate the oxidation state of metals in structures stored in the CSD (using methods described in ref 11). This program uses two methods, ligand template matching and bond valence sums (BVS), to calculate metal oxidation state. Ligand template matching attempts to identify all ligands bonded to a metal, define the charge on each ligand, and hence deduce the metal oxidation state based on the sum of the ligand charges and the overall charge on the complex. At present the program has 250 ligand templates defined, and, in cases where the ligand cannot be identified, the program allows the user to assign the oxidation state of the ligand or the metal itself manually. The use of BVS is based on the bond valence model,[14] which is the most widely used means of assigning oxidation states from bond length data. The BVS for atom *i* is the sum (eq 2) over all bonds to atoms *j* of the individual bond valences, S_{ij}. The S_{ij} are calculated using the expression in eq 3.

$$\mathrm{BVS} = \Sigma S_{ij} \tag{2}$$

$$S_{ij} = \exp[(R_o - R_{ij})/B] \tag{3}$$

Here R_{ij} is the experimentally determined M−L bond length, and B and R_o are constants. B in OXQUEST has the widely used value of 0.37,[15] while oxidation-state independent R_o values derived by Palenik and co-workers[16−18] are used for most metals; in other cases they are derived from atomic parameters,[19] except for copper, where oxidation state dependent R_o values are used as derived by Shields et al. by an iterative process.[11]

In all cases studied here, metal oxidation states were assigned using OXQUEST. The assignment of oxidation state by the program is automatic if the ligand template matching and BVS methods agree; however, as discussed below, BVS values are not reliable indicators of metal oxidation states for all structures. Particularly for the tertiary phosphine and Rh−alkene examples (Table 1), the BVS values were clearly wrong for many structures, and the ligand template method was used for calculation of oxidation state. For all M−L groups studied, there were a few entries where there was manual assignment of oxidation state due to both methods being unsuccessful. On those rare occasions when the oxidation state was difficult to determine or the species is of mixed-valence, the structure was excluded from the analyses below.

Metal Coordination Number. For each metal atom in the complexes studied a coordination number was assigned using OXQUEST according to the algorithm used in the 1989 Dalton table.[1a] This takes into account the number of coordination sites occupied by multihapto and bridging ligands, rather than simply counting the total number of ligand atoms within bonding distance of the metal. For example, η^5-ligands (e.g. cyclopentadienyl) and η^6-benzene ligands are assigned to occupy three coordination sites rather than five or six, respectively. Further details are given in the Dalton paper.[1a]

Spin State. Metal spin states are not searchable in the CSD. Some entries record that the complex is high or low spin, but this is not consistently available for all affected entries. Procedures are therefore required to enable (automatic) identification of cases where the metal spin state is potentially unpredictable or controversial. These effects are only likely to be significant for first transition series metals [Co(II, III), Fe(II, III), Cr(II), Mn(II, III)] with coordination numbers 5 or 6. Therefore for the M−L systems listed in Table 1 only Co, Fe, and Mn fragments were analyzed for spin effects. As low-spin fragments have shorter M−L bond lengths than their high-spin counterparts, it should be possible to assign spin state if a bimodal distribution is obtained for a given metal oxidation state and ligand. However, if the metal can also show Jahn−Teller effects (see below), or the distribution is not clearly bimodal, or there are only one or two outliers, it is much harder to assign spin states reliably.

Jahn−Teller Effect. Jahn−Teller effects are not explicitly addressed in the CSD despite their dramatic influence on bond lengths in certain well-known cases. As for spin, there is no easy way to identify Jahn−Teller effects from geometry alone. Again they are only likely to be significant for a limited number of first row transition metals of particular oxidation and spin states and coordination number. These are as follows: 5- or 6-coordinate Cu(II), low-spin Co(II) and Ni(III), high-spin Cr(II) and Mn(III) (see for example, the review by Falvello[20]). In the examples reported below,

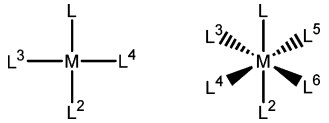

Figure 1. L^2 trans to M−L bond ($L-M-L^2 \geq 150°$) for 4-coordinate square-planar and 6-coordinate octahedral complexes.

therefore, Cu(II)−OH_2 and Mn(III)−Cl bond lengths were analyzed for Jahn−Teller effects.

Metal Coordination Geometry. The main metal coordination numbers examined in this study are 4−7. Six-coordinate metals are overwhelmingly of octahedral geometry (but see ref 23) and particularly so in the systems studied in the present work, so no division on 6-coordinate geometry was applied. For 4, 5, and 7 coordination there are a number of possible geometries.

We note that there are various methods to assign and analyze geometry for a range of coordination numbers. Alvarez and co-workers have recently published detailed analyses of 4-, 5-, 6-, and 7-coordinate geometries using continuous shape and symmetry measures.[21−24] Raithby et al. have used symmetry deformation coordinates and principal component analysis to analyze the 4-coordinate geometries of Cu complexes.[25] Allen and co-workers[26] have shown how a Euclidean dissimilarity metric can be used to quantify the angular distortion of a ML_n ($n = 4-7$) species from an archetypal geometry.

In this study we have investigated the effect of variation in 4-coordinate geometries and subdivided them into square planar, tetrahedral, disphenoidal (sawhorse), and "distorted" (see below). These geometries were assigned on the basis of L−M−L angles: structures were deemed square planar when two angles (L^1-M-L^2, L^3-M-L^4) were ≥ 150°; tetrahedral when all L−M−L were ≤ 140°; disphenoidal when one angle L^1-M-L^2 was ≥ 150°; and another L^3-M-L^4 was ≤ 130° and as distorted if not one of these types. We note the prospect of using more flexible and continuous descriptors such as those cited above[21−26] of coordination geometry in future implementations of the ideas studied in this paper.

Pentacoordinate geometries were not further categorized, except in the case of Mn−Cl, because of the continuum of geometries that exists between the archetypes. Similarly, no subdivision of 7-coordinate geometries was attempted.

Trans Influence. Trans influence (also termed the structural trans effect) is a well-known and important phenomenon, particularly for *d*-block metals.[27,28] It may be defined as the ability of a ligand to influence the length of the $M-L^2$ bond trans to it (Figure 1). The trans influence depends on the metal coordination type, its d-electron configuration, and the ligands, L and L^2. In this work, therefore, we have divided bond length distributions according to the ligand, L^2. In general, we have considered only the contact atom type of L^2 rather than ligand type, except for carbon ligands where σ-bonded and π-bonded C ligands were dealt with separately. For L^2 = O, N, P, S, halogen (F, Cl, Br, I), or σ-C, L^2 was defined as trans to the M−L bond when the L^2-M-L angle was ≥ 150°. For η^2-alkenes, this angle was considered to be defined by the midpoint of the η^2-C═C alkene bond. For M−L fragments of metal coordination number = 5, 6, or 7 with a η^5-Cp, η^6-arene, or derivative bonded to M, the η-bonded ligand was defined as being trans to all the other metal−ligand bonds. For Pd−Cl allyl complexes, the "trans" ligand was considered to be defined by the central allyl carbon atom. Finally, cases were assigned where the ligand, L, is not trans to any other ligand, as identified by all $L-M-L^2$ angles being less than 150°.

Statistics. All mean bond lengths and SSDs quoted in this paper were generated by the Vista program of the CSD software system.[2] The mean values, *d*, quoted are the unweighted sample means, and the SSD values, σ, were calculated according to eq 4 below

$$\sigma = [\sum_{i=1}^{n}(d_i - d)^2/(n-1)]^{1/2} \quad (4)$$

in which d_i is the *i*th observation of the bond length in a sample of *n* observations.

For each M−L group, the initial data set was checked for outliers that were more than 4σ from the sample mean. In the small number of cases where on close examination of the data there appeared to be an error in the structure, the outliers were removed from the data set and the mean and SSD recalculated.

In the tables below, the mean (*d*), SSD, and number of M−L fragments in the data set are given in the format: mean (SSD) number of fragments. Mean values are tabulated for a particular oxidation state or metal coordination number if there are 5 fragments or more in the data set, and these fragments arise from at least 3 different crystal structures. Mixed valence or partially oxidized fragments are not listed in the tables, or cases where oxidation state was difficult to assign, for example in some boron cage complexes. For the subdivision by trans ligand, only the most common trans ligands are listed (generally data sets with 10 or more observations).

Metals. Metals were chosen so as to provide representative examples from all three series of the *d*-block (i.e. groups 3−12 of the periodic table) and to include metals which are known to have large variations in bond lengths and geometries (Hg and Cu) but which had reasonable numbers of structures in the CSD.

Ligands. The 6 ligands reported here (Table 1) were chosen to include hard ligands (carboxylates, chlorides, and water), found mainly in coordination complexes, and soft ligands (phosphines and alkenes), which form more "organometallic" complexes, as well as those of intermediate character such as pyridines. For the carboxylates, the three main binding modes (monodentate, chelating, and bridging, each O bonded to one metal only) (Figure 2) were analyzed (see ref 8 for a more comprehensive and detailed study). For the other ligands, only the main bonding mode was studied, i.e. terminal chlorides, pyridines, water and phosphines and η^2-bonded alkenes. The carboxylate, pyridine, phosphine, and alkene submolecular fragments searched for in the CSD are defined in Figure 2. For the carboxylate searches the requirement of nonmetal atoms having a coordinate *exactly* as shown prevents diolates, etc. from being located. For the Rh−alkene search, no direct link between Rh and C_α atoms was allowed and the CC bond was specified as either single or double and $C-C_\alpha$ bonds as single, so as to eliminate larger π-bonded ligands such as butadienes

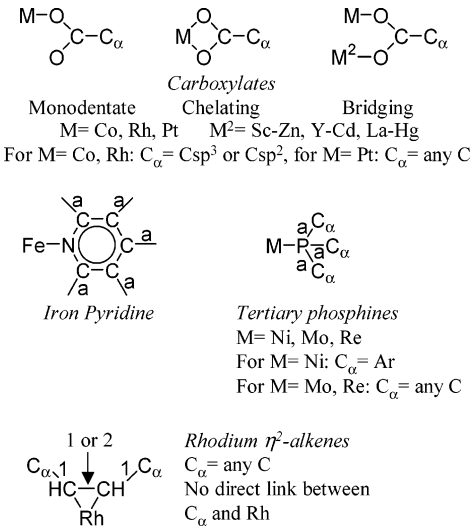

Figure 2. Search fragments for carboxylate, pyridine, tertiary phosphine, and alkene complexes. All bonds were set to be of "any type" except for Rh−alkene fragments (see text). Nonmetal atoms have coordination exactly as shown, except C_α atoms. Acyclic bonds are marked with 'a'.

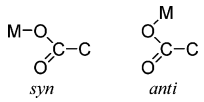

Figure 3. The syn and anti conformations of monodentate carboxylate ligands.

(Rh−C bonds were defined as 'any type'). Throughout this study, 'R' specifies an alkyl group and 'Ar' an aryl group.

RESULTS AND DISCUSSION

Carboxylate Complexes.[8] Carboxylate ligands in monodentate, chelating, and bridging modes (Figure 2) in Co, Rh, and Pt complexes were analyzed. Mean M−O bond lengths, SSDs, and number of fragments are given in Table 2. For these metals OXQUEST successfully assigned the metal oxidation state in more than 90% of all fragments (the oxidation state was assigned by hand in the remaining cases). The C−C bond of the carboxylate ligand was classified as either cyclic or acyclic (as defined in the 1989 Dalton tables).[1a] For Co and Rh the distributions were divided according to the hybridization of the carbon to which the carboxyl group is attached. No distinction was made between anti and syn conformations of the ligand (see Figure 3). The first subdivision was on whether the metal−carboxylate fragment is part of a metal cluster, i.e. whether the Co, Rh, or Pt metal is bonded to two or more metals. Mean M−O bond lengths for metal clusters are only given for bridging Co−O_2CC (sp^3) and the Pt−carboxylates in Table 2. For all other carboxylate fragments there are none or only one or two metal cluster structures.

Figure 4 shows a histogram of Co−O bond lengths for all 619 monodentate Co−O_2C−C (sp3) fragments (cf. in the 1989 tables there were 195 observations). The mean Co−O distance is 1.929 (62) Å, and the histogram is clearly bimodal. Figure 4 illustrates how the Co−O bond lengths can be subdivided to give data sets which are more chemically well-defined with sharper distributions with smaller SSDs. On dividing the fragments according to the cobalt oxidation state, Co(II) and Co(III) data give unimodal histograms with Co(III) showing a substantial reduction in SSD. The difference in mean Co−O bond length between Co(II) and Co(III) is quite large (0.145 Å) and is in the expected[1a] direction with d[Co(II)−O] > d[Co(III)−O]. Some further division is then possible. In the case of Co(III), all the examples are 6-coordinate, but for Co(II) there are a few 4- and 5-coordinate cases and, although the number of fragments is small, the mean Co−O bond length increases from 4- to 6-coordinate Co(II) by ca. 0.1 Å (Table 2). This is in fair agreement with the conclusions of See and coworkers[7] that the mean difference in M(II)−L bond lengths (M = Mn, Fe, Co, Ni, Cu, Zn) between octahedral and tetrahedral geometries is 0.14 Å. Finally, for the octahedral complexes the Co−O bond lengths were divided according to the ligand trans to the Co−carboxylate bond. This resulted in a small difference in the mean Co(III)−O bond lengths (0.015 Å) with Co−O bonds trans to N being slightly longer and both O and N data sets having reasonably small SSDs. For the 6-coordinate Co(III) fragments there is one Co−O bond length (2.059 Å) more than 4σ from the mean (1.904 (20) Å). This Co(III)−O bond is trans to a σ-bonded carbon ligand and is the only example of a Co−carboxylate bond trans to C in the Co (III) data set. The mean Co−O bond lengths for monodentate O_2CC (sp^2) ligands are also tabulated and show no significant differences from lengths for O_2CC (sp^3) ligands.

The number of chelating Co−carboxylates is relatively small, and the SSDs on Co−O lengths are large for both O_2CC(sp^2) and O_2CC(sp^3). Some of the carboxylate fragments are asymmetric with one short Co−O bond (∼2.1 Å) and one longer bond (∼2.4 Å). Removing asymmetric chelating carboxylates where the difference in the two Co−O bond lengths is greater than 0.2 Å gives more reasonable SSDs.

For bridging Co carboxylates, a similar division of structures was performed. For bridging O_2CC(sp^2) carboxylates the SSDs remain relatively high for all divisions of data. However for bridging O_2CC(sp^3) carboxylates there is a reduction in SSDs on subdivision of the distribution. As for monodentate carboxylates, there is a difference in Co(II)−O bond lengths between 4- and 6-coordinate complexes of 0.114 Å. There is no significant difference in mean Co−O bond lengths for monodentate versus bridging carboxylates. There are few outliers, consistent with all these complexes being high spin with no significant Jahn−Teller effects.

Rhodium carboxylate fragments were treated in essentially the same way. In this case there were only a few monodentate O_2CC(sp^3) carboxylates (54 fragments) but a large number of bridging carboxylates, with many taking the form [Rh_2(μ-O_2CR)$_4$L′$_2$]. This may explain the reasonably small SSD for Rh(II), 6-coordinate fragments with O trans (Rh−O: 2.037 (14) Å) since all such complexes would contribute to this category of bond lengths. In comparison, Rh−O carboxylate bond lengths with trans P or C ligands are longer and have larger SSDs (2.142 (28) Å and 2.193 (25) Å, respectively). The effect on Rh−O bond lengths of the trans ligand leads to the Rh(II) distribution having one sharp peak corresponding to the structures with O trans and a smaller number of bond lengths in a broad distribution with a number lying more than 4σ from the mean. These are from carboxylates trans to P or C ligands. As in the cobalt case, there are only a few chelating carboxylates and again some are asymmetric.

Table 2. Mean M−O Bond Lengths (Å) for Monodentate, Chelating, and Bridging Co, Rh, Pt Carboxylates[b]

M−O_2CC	total fragments	oxidation state	metal coordn no. (geometry)	trans ligand
Co−O_2CC(sp^3)				
monodentate	1.929 (62) 619	Co(II): 2.049 (58) 103	4: 1.973 (21) 18	
			all tetrahedral	
			5: 1.981 (44) 8	
			6: 2.073 (42) 74	O: 2.074 (32) 60
		Co(III): 1.904 (20) 514	all 6 coordinate	N: 1.910 (15) 257
				O: 1.895 (17) 234
chelating	2.107 (123) 32	Co(II): 2.127 (117) 28	5: 1.988 (10) 8	
	2.081 (103) 26[a]	Co(II): 2.103 (96) 22[a]	5: 1.988 (10) 8[a]	
			6: 2.183 (90) 20	
			6: 2.169 (42) 14[a]	
bridging	2.023 (79) 230			
		metal clusters: 2.017 (69) 18		
		Co(II): 2.053 (56) 165	4: 1.962 (29) 16	
			all tetrahedral	
			5: 2.019 (57) 34	
			6: 2.076 (37) 114	O: 2.079 (37) 79
		Co(III): 1.892 (23) 36	all 6 coordinate	O: 1.887 (23) 29
Co−O_2CC (sp^2)				
monodentate	1.944 (67) 177	Co(II): 2.066 (50) 34	6: 2.079 (32) 31	all trans to O
		Co(III): 1.915 (24) 143	all 6 coordinate	N: 1.913 (15) 106
				O: 1.893 (15) 20
chelating	2.190 (97) 40	all Co(II)		
	2.175 (41) 28[a]			
bridging	2.065 (64) 108	Co(II): 2.070 (58) 98	5: 2.016 (54) 11	
			6: 2.078 (54) 86	O: 2.071 (56) 53
				N: 2.094 (61) 9
Rh−O_2CC (sp^3)				
monodentate	2.059 (61) 54	Rh(I): 2.059 (12) 11	all 4 coordinate, square planar	
		Rh(III): 2.060 (70) 39	all 6 coordinate	N: 2.028 (39) 18
				O: 2.020 (20) 11
				η^5/η^6-C ligands: 2.103 (22) 9
chelating	2.211 (116) 19			
	2.194 (42) 13[a]			
bridging	2.056 (47) 673	Rh(I): 2.104 (17) 20	4: 2.097 (9) 16	
			all square planar	
		Rh(II): 2.053 (44) 576	5: 2.044 (37) 8	
			6: 2.053 (44) 568	σ-C: 2.193 (25) 27
				O: 2.037 (14) 506
				P: 2.142 (28) 41
		Rh(III): 2.040 (43) 28	6: 2.040 (43) 28	O: 2.027 (21) 25
Rh−O_2CC (sp^2)				
monodentate	2.060 (33) 32	Rh(I): 2.056 (23) 13	all 4 coordinate, square planar	
		Rh(III): 2.063 (40) 18	all 6 coordinate	η^5/η^6-C ligands: 2.088 (18) 12
chelating	1 hit only			
bridging	2.047 (28) 48	Rh(I): 2.101 (21) 8	all 4 coordinate, square planar	
		Rh(II): 2.037 (12) 40	6: 2.037 (12) 36	
Pt−O_2CC				
monodentate	2.027 (43) 267			
		metal clusters: 2.123 (85) 11		
		Pt(II): 2.030 (34) 165	all 4 coordinate, square planar	N: 2.018 (22) 104
				O: 2.019 (26) 27
				P: 2.071 (19) 32
		Pt(IV): 2.009 (33) 87	all 6 coordinate	halogen: 2.026 (22) 10
				N: 2.010 (20) 22
				O: 1.999 (22) 54
chelating	no hits			
bridging	2.054 (59) 117		.	
		metal clusters: 2.051 (63) 63 all Pt(II)	all 6 coordinate	M: 2.143 (32) 18
				O: 2.015 (18) 45
		Pt(II): 2.052 (37) 39	4: 2.050 (36) 33 all square planar	N: 2.042 (24) 25

[a] Chelating carboxylate fragments with difference in M−O bond lengths > 0.2 Å removed from data set. [b] The mean (*d*), SSD, and number of M−L fragments in the data set are given in the format: mean (SSD) number of fragments.

A more reasonable SSD is obtained if these are removed. This would imply that an automated algorithm should detect and treat separately asymmetric chelating (and bridging ligands). The number of O_2CC(sp^2) ligands is small, but they show mean Rh−O bond lengths very similar to O_2CC(sp^3) values. The Rh−O bond lengths for bridging sp^2 and sp^3

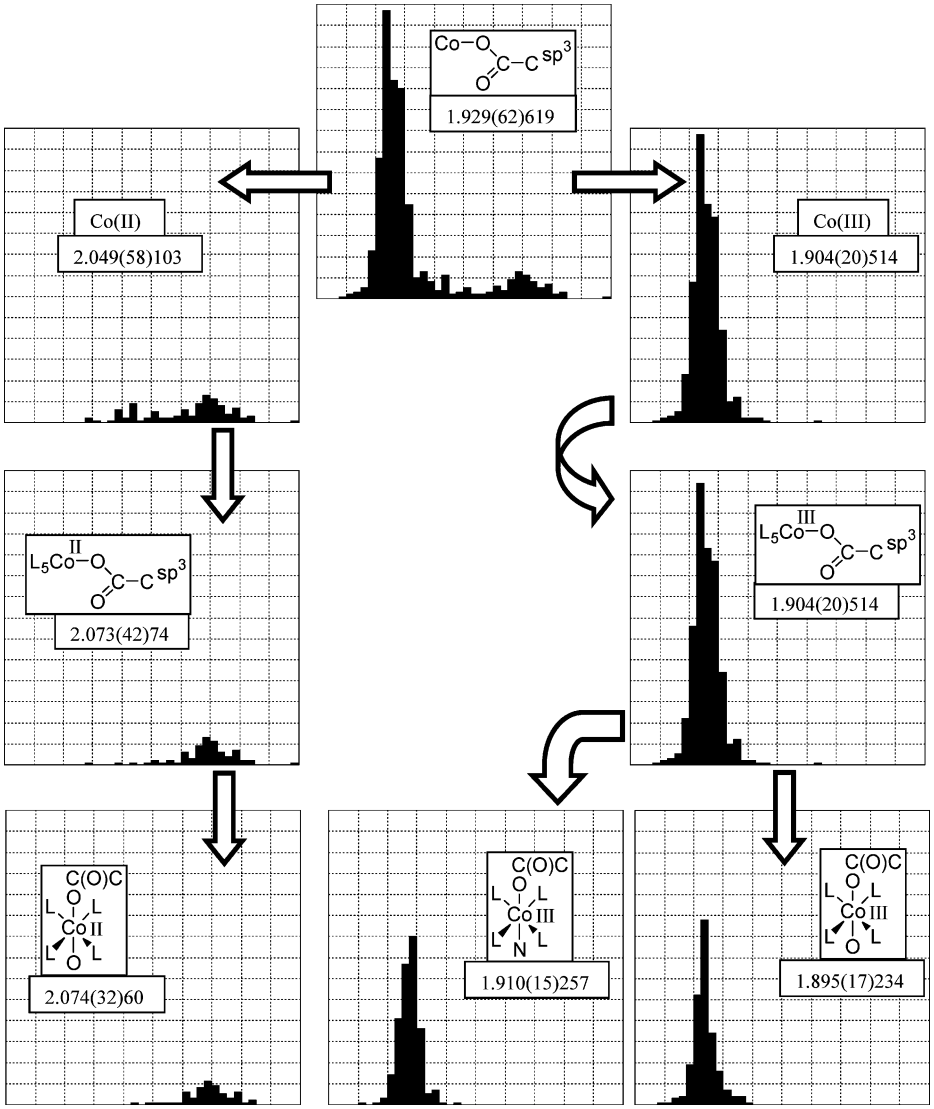

Figure 4. Histograms for 619 monodentate Co−O_2CC(sp^3) bond lengths upon division by oxidation state, metal coordination number, and ligand trans to Co-carboxylate bond.

carboxylates of 4-coordinate Rh(I) fragments are longer (by 0.042 Å on average, see Table 2) than the equivalent monodentate carboxylate fragments.

Finally in Table 2, mean bond lengths are reported for platinum carboxylates. In this case no distinction was made between sp^2 and sp^3 substituents, but otherwise the analysis was the same as for Co and Rh. Reasonable SSDs (ca. 0.02 Å) are obtained for Pt−O data sets if the fragments are divided on oxidation state, metal coordination number, and ligand trans to the Pt−O bond. There is one Pt−O bond length more than 4σ from the mean for both Pt(II) and Pt(IV) monodentate carboxylates. In both cases the Pt−O bond is trans to a C ligand, there being no other examples in the data set (vide supra, Co(III) monodentate carboxylates). In her CSD study[4] of metal carboxylates for a range of metals that are commonly found in metalloproteins, Harding reports SSDs of ca. 0.07 Å for the full data sets, close to values reported here.

Chloride Ligands. Table 3 lists statistics for M−Cl bond lengths for Cl terminally coordinated to Fe, Hg, Mn, and Pd. A histogram of Fe−Cl bond lengths for all Fe−Cl fragments is shown in Figure 5. The distribution is bimodal with a mean Fe−Cl bond length of 2.242 (68) Å. Figure 5 shows how the Fe−Cl bond length distribution can be subdivided in a similar way to the metal−carboxylate system. First, a few metal cluster structures were removed (many of which have mixed valence Fe). In contrast to the Co−O_2-CC (sp^3) system (see Figure 4), division by oxidation state does not give unimodal distributions; however, subsequent division by metal coordination number provides unimodal histograms and substantially reduced SSDs. Fe−Cl bonds for 4-coordinate tetrahedral iron are shorter than those for 6-coordinate complexes with a difference in mean bond lengths of 0.084 Å for Fe(II) and 0.119 Å for Fe(III). For the 6-coordinate Fe−Cl complexes, some further reduction in SSD is possible by division on the atom trans to the Fe−Cl bond. For the tetrahedral Fe(III)−Cl fragments a large majority (291 fragments) are $[FeCl_4]^-$ with a mean Fe−Cl bond of 2.179 (17) Å. There are no outliers in any of these distributions to suggest any substantial spin state effects; complexes are likely to be high spin. However, for 5-coordinate Fe(III)−Cl fragments there are a few complexes with intermediate spin state ($S = 3/2$) or of mixed high and intermediate spin. The intermediate and mixed spin species

Table 3. Mean Fe, Hg, Mn, and Pd−Cl Bond Lengths (Å) for Terminal Cl Ligands

M-Cl	all fragments	oxidation state	metal coordn no.	Jahn−Teller effect	metal coordn geometry	trans ligand	$[MCl_x]^{n-}$
Fe−Cl	2.242 (68) 866	metal clusters: 2.224 (24) 63					
		Fe(II): 2.314 (59) 125	4: 2.281 (35) 62		all tetrahedral		$[FeCl_4]^{2-}$: 2.306 (19) 31
			5: 2.283 (34) 16				
			6: 2.365 (47) 46			halogen: 2.376 (46) 18 η^5/η^6-C ligands: 2.316 (24) 6 σ-C: 2.344 (38) 9	
		Fe(III): 2.230 (64) 673	4: 2.189 (24) 407		all tetrahedral		$[FeCl_4]^{-}$: 2.179 (17) 291
			5: 2.247 (43) 62				
			6: 2.308 (48) 190			halogen: 2.360 (46) 29 N: 2.288 (37) 106 O: 2.319 (41) 52	
			7: 2.302 (56) 14				
Hg−Cl	2.401 (109) 557	metal clusters: 2.434 (92) 7					
		Hg(I): 2.380 (25) 4					
		Hg(II): 2.401 (109) 540	2: 2.319 (24) 90			halogen: 2.289 (10) 10	
			3: 2.333 (34) 40				
			4: 2.430 (102) 343		disphenoidal, Cl axial[a]: 2.325 (34) 66 max Cl−Hg−L 140−150°: 2.347 (28) 30 tetrahedral[b]: 2.455 (67) 227 disphenoidal, Cl eq.[c]: 2.694 (111) 16		$[HgCl_4]^{2-}$: 2.482 (52) 86
			5: 2.378 (48) 36 plus 5 fragments: 2.650−3.029			halogen: 2.347 (33) 10	
			6: 2.330 (20) 12 plus 2 fragments: 2.505, 2.769				
			8: 2.323 (20) 7				
Mn−Cl	2.399 (88) 252	Mn(I): 2.383 (16) 16					
		Mn(II): 2.418 (80) 174	4: 2.352 (23) 73		all tetrahedral		$[MnCl_4]^{2-}$: 2.359 (16) 56
			5: 2.369 (46) 25				
			6: 2.494 (49) 71			halogen: 2.514 (33) 31 N: 2.443 (30) 19 O: 2.509 (51) 20	
		Mn(III): 2.357 (102) 58	5: 2.362 (54) 27		tet. pyramidal: 2.384 (28) 20 Tbp: 2.298 (60) 7		
			6: 2.352 (131) 31	<2.4 Å: 2.260 (30) 20 >2.4 Å: 2.519 (41) 11			
Pd−Cl	2.333 (53) 1295	metal clusters: 2.380 (46) 10					
		Pd(I): 2.399 (36) 37	4: 2.397 (36) 35		all square planar		
		Pd(II): 2.330 (52) 1215	4: 2.328 (40) 1200		all square planar	halogen: 2.298 (15) 254 N: 2.301 (18) 276 O: 2.289 (17) 11 P: 2.358 (17) 187 S: 2.325 (18) 132 σ-Csp[1]: 2.307 (25) 22 σ-Csp[2]: 2.395 (23) 114 σ-Csp[3]: 2.400 (28) 41 η^2-alkene: 2.319 (19) 48 η^3-allyl: 2.378 (14) 23	$[PdCl_4]^{2-}$: 2.306 (10) 48
			5: 2.512 (269) 13 >4σ removed: 2.376 (58) 10				
		Pd(IV): 2.333 (56) 11	all 6 coord				

[a] (I) (Figure 6): Max Cl−Hg−L > 150°, L′−Hg−L′ < 120°. [b] (II): all Cl−Hg−L, L−Hg−L < 140°. [c] (III): Cl−Hg−L < 120°, L′−Hg−L′ > 144°.

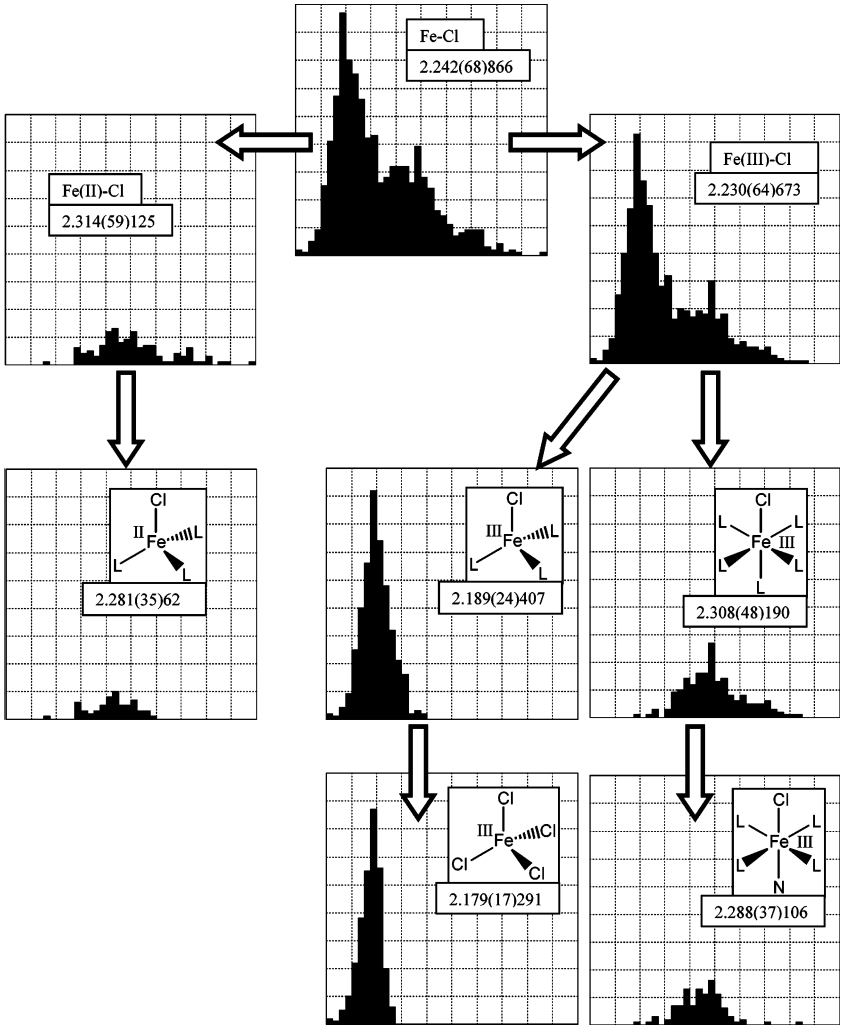

Figure 5. Histograms of all 866 terminal Fe−Cl bond lengths upon division by oxidation state, metal coordination number, and trans ligand to Fe−Cl bond.

tend to have a longer Fe−Cl bond length (>2.50 Å) compared to the high-spin complexes. However, it is not possible to identify the spin state from the Fe−Cl bond lengths, as there is a unimodal distribution for the 5-coordinate Fe(III)−Cl data set with no outliers (cf. iron−pyridine fragments below). Therefore, in such a case, the distribution could be flagged that there are unresolved spin state issues for these complexes, to be addressed in future versions of the molecular geometry library.

The bond length SSDs of 0.017 Å and 0.019 Å for the Fe−chloride anions $[FeCl_4]^-$ and $[FeCl_4]^{2-}$, respectively, are in good agreement with our previous general[9] analysis of M−L bond lengths and our analysis of bond lengths in complex ions,[10] where $[FeCl_4]^-$ and $[FeCl_4]^{2-}$ are two of the more well-behaved anionic species. By comparison, Hg−Cl bond lengths are more easily deformed.[10] Table 3 shows the division of Hg−Cl bond lengths in a similar way to that attempted for Fe. The SSD for all Hg−Cl fragments is very high (0.109 Å) with a positively skewed distribution. Division by oxidation state and coordination number gives quite reasonable SSDs for Hg(II) with coordination numbers 2 and 3. The 5- and 6-coordinate mercury species give acceptable SSDs if a few long bonds are excluded. This raises the issue of bond length cutoff noted above. However 4-coordinate Hg(II) species of the form $HgClL_3$ have a high SSD (0.102 Å) with a wide range of Hg−Cl bond lengths. Disphenoidal

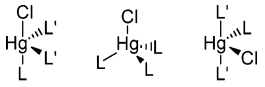

Figure 6. Coordination geometries for 4-coordinate Hg(II)−chloride species: (i) disphenoidal, Cl axial; (ii) tetrahedral; (iii) disphenoidal, Cl equatorial.

(i, iii) and tetrahedral(II) coordination geometries (see Figure 6) occur. There is a correlation, as shown in Figure 7, between the maximum Cl−Hg−L angle and the Hg−Cl bond length, such that the larger the angle the shorter the Hg−Cl bond.[29] This is consistent with division by Hg geometry giving a reasonable division of the data. The shortest bond lengths are for (I), the disphenoidal geometry with Cl in an axial position (Cl−Hg−L: ≥ 150°, L′−Hg−L′: 50°−108°), with mean Hg−Cl of 2.325 (34) Å. There is an intermediate, "distorted" (see Table 3) geometry group with maximum Cl−Hg−L between 140° and 150° (Hg−Cl: 2.347 (28) Å). Next, the tetrahedral geometry (II) in which all L−Hg−L and Cl−Hg−L angles are less than 140°, has mean Hg−Cl 2.455 (67) Å. This tetrahedral group incorporates all $[HgCl_4]^{2-}$ species [mean bond length of 2.482 (52) Å] (much higher SSD than for Fe species, as noted previously[10]). The disphenoidal complexes with Cl in an equatorial position (III) (Cl−Hg−L: 86° to 115°; L′−Hg−L′: >144°) have the

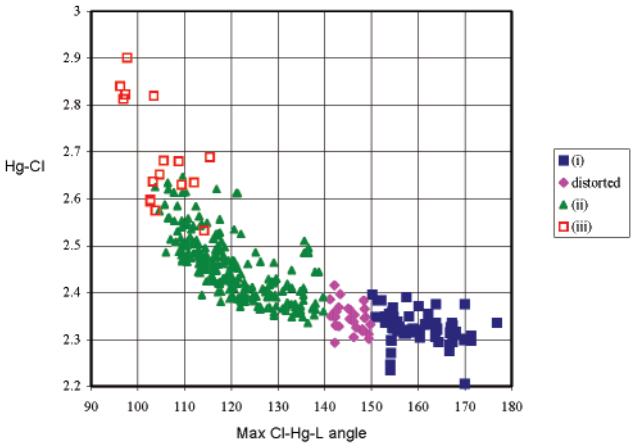

Figure 7. Scatter plot of maximum Cl−Hg−L angle vs Hg−Cl bond length for 4-coordinate Hg(II)−Cl species. See in Figure 6 for definitions of (i), (ii), and (iii); 'distorted' corresponds to maximum Cl−Hg−L in range 140°−150°.

longest Hg−Cl bonds and largest SSD (2.694 (111) Å). There are also 4 'square planar' structures in the data set with short Hg−Cl bond lengths (~2.305 Å). Three of these structures are better described as 6-coordinate with long Hg−O/N/Cl bonds. The other is coded in the CSD as a $HgCl_2$ dimer, but, due to recalculation of Hg−Cl connectivity, two long Hg−Cl bonds are now included so it is now defined as 4-coordinate. These cases show the importance (and problems) of standardizing bond connections for certain metals, and that it can be difficult to obtain bond connections which are appropriate for all structures. Nevertheless, this study shows that, even for soft, easily deformed systems such as Hg−Cl, comparatively reasonable SSDs are forthcoming from careful division of data on oxidation state, coordination number, and metal coordination geometry.

The third example in Table 3, Mn-Cl, shows larger SSDs than the Fe−Cl system. This is at least in part due to Jahn−Teller and, possibly, spin effects. The Mn(II)−Cl fragments are reasonably well-behaved. Thus, tetrahedral $[MnCl_4]^{2-}$ anions have a SSD of 0.016 Å, and the difference in Mn−Cl bond lengths for 4-coordinate versus 6-coordinate Mn is 0.142 Å. However, d^4 Mn(III) 6-coordinate complexes have a bimodal distribution due to spin or, more likely, Jahn−Teller effects (see iron−pyridine discussion below) with a large SSD (0.131 Å). This data set can be split into two distinct groups of Mn−Cl bonds, respectively shorter and longer than 2.4 Å. It was possible to divide 5-coordinate Mn(III)−Cl fragments into tetragonal pyramidal and trigonal bipyramidal subsets by examination of L−Mn−L angles. For all the tetragonal pyramidal structures, the Cl ligand is in the apical position and thus not trans to any ligand. For the few tbp structures, the shortest Mn−Cl bond is where the Cl is in an axial position and thus trans to another ligand, while the other Mn−Cl fragments are in equatorial sites. It is not clear whether these Mn−Cl bonds are also influenced by Jahn−Teller effects, although three of the tetragonal pyramidal structures have Mn−Cl bonds slightly longer than 2.4 Å.

Finally, Pd−Cl fragments were analyzed (see Table 3). These, as one might expect, are mainly square planar Pd(II) species. They show smaller variation in the Pd−Cl bond length with significant trans influence effects, as shown in Table 3. Thus, subdivision by trans ligands leads to reasonable SSDs. However, there are three Pd−Cl bond lengths (2.831 Å, 2.956 Å, and 3.106 Å) more than 4σ from the mean in the complete data set. These are all due to 5-coordinate Pd(II) species, with the long Pd−Cl bond in the apical position of tetragonal pyramidal geometry. This is reflected in the large SSD for the few 5-coordinate Pd(II) fragments (Table 3). These are therefore not erroneous but representative of a relatively rare subset of structures.

Copper Complexes. The structural chemistry of copper complexes has been extensively studied using the CSD (see for example Raithby et al.[25] and references therein), and it is well-known that copper(II) d^9 complexes are deformed by Jahn−Teller effects. This is apparent in the Cu−OH_2 distributions shown in Figure 8 and Table 4.

As one might expect, the distribution of Cu−O bond lengths (Figure 8) is very broad and bimodal, with one sharp peak at 1.95 Å, a broad peak from 2.1 Å to 2.8 Å, and a SSD of 0.224 Å. Nearly all the Cu−OH_2 species are Cu(II), with only 10 Cu(I) complexes present (which are all 3-coordinate or tetrahedral 4-coordinate). For Cu(II), there are only a few (27) 4-coordinate Cu species, and these are all square planar, with a reasonably low SSD (0.031 Å) in the absence of a Jahn−Teller effect. Both 5- and 6-coordinate Cu(II)−OH_2 fragments have bimodal bond length distributions (Figure 8), with the shorter class of distance having Cu−O < 2.1 Å and long (Jahn−Teller affected) Cu−O bonds > 2.1 Å.

For 5-coordinate Cu complexes almost all the shorter Cu−O bonds have a ligand trans to the Cu−OH_2 bond (in most cases O or N). The group of longer Cu−O bonds has no trans ligand (i.e. no O−Cu−L^2 bond angle > 150°). As shown in Figure 8, this corresponds to a geometry with either the water ligand in the apical site of a tetragonal pyramid or in an equatorial site for an approximately tbp structure. All the Cu−OH_2 bond lengths with trans O or N ligands are shorter than 2.1 Å with mean SSDs approximately 0.030 Å. The 522 5-coordinate Cu−OH_2 fragments with no trans ligand to OH_2 have bond lengths ranging from 1.932 Å to 2.797 Å, with only 24 Cu−OH_2 bonds above 2.55 Å. Only 18 of the fragments have a Cu−O bond shorter than 2.1 Å.

For the 6-coordinate complexes, as one would expect, there is a wide bond length distribution although the proportion of short and long Cu−O bonds varies with the trans ligand. For trans N ligands, only 12% of Cu−OH_2 bonds are longer than 2.1 Å, while for trans O ligands, 65% of Cu−OH_2 bond lengths are over 2.1 Å; all Cu−OH_2 bonds trans to metals are longer than 2.1 Å. The 6-coordinate Cu−OH_2 histogram in Figure 8 is similar to that reported by Harding in her study.[4] In comparison, M−OH_2 bond lengths for Ca, Mg, Fe, and Mn were shown by Harding[4] to have unimodal distributions with SSDs of between 0.03 Å and 0.06 Å.

There are 11 $[Cu(OH_2)_6]^{2+}$ species in the data set, which have a mean Cu−O bond length of 2.106 Å with a SSD of 0.198 Å. This bimodal distribution may be divided into short [1.966 (18) 24 Å] and long [2.366 (64) 13 Å] bond length distributions.

Although not reported in this paper we found distributions for Cu−carboxylates to be very similar to those for Cu−OH_2, with a similar cutoff point apparent between short and long Cu−O bonds at 2.1 Å. The mean Cu−O bond lengths for monodentate and bridging carboxylates are slightly shorter than for Cu−OH_2. In particular, for the 5-coordinate

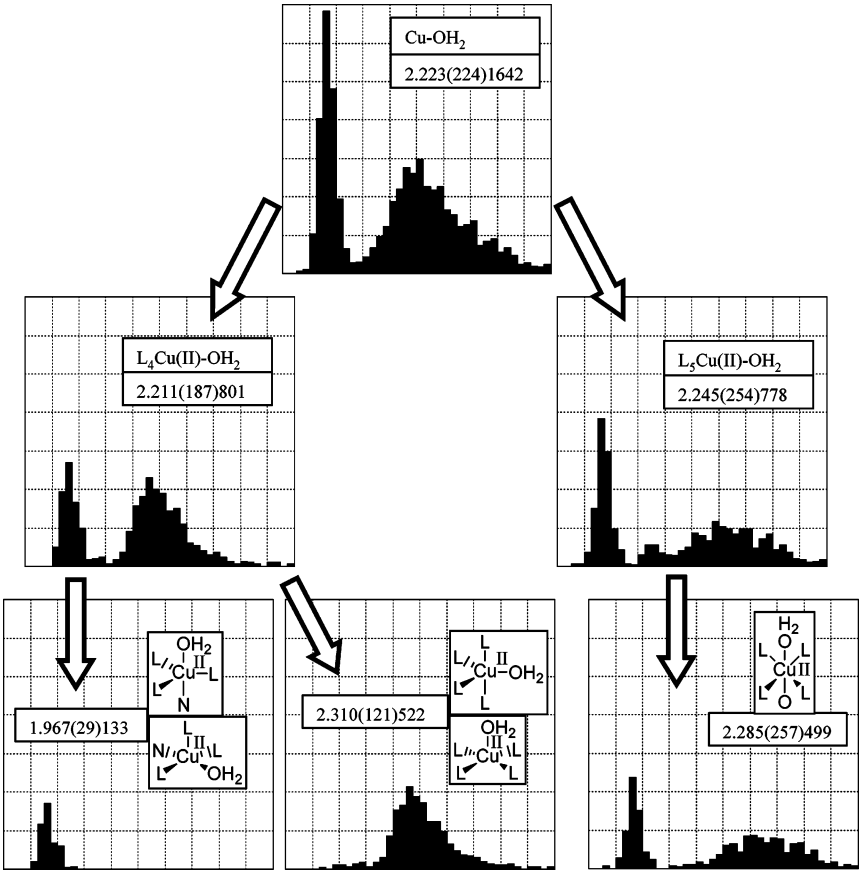

Figure 8. Histograms of 1642 terminal Cu−OH_2 bond lengths upon division by metal coordination number, ligand trans to Cu−O bond and Cu−O bond not trans to any ligand.

Cu−carboxylate bond lengths the percentage of long Cu−O bonds is much smaller than that found for 5-coordinate Cu−OH_2 complexes. Harding[4] also reports on Cu−carboxylates with short Cu−O bond lengths in the range 1.91−2.03 Å.

Iron−Pyridine Fragments. For the Co−carboxylate and Fe−chloride data sets, as noted above, there appears to be no significant spin state effects on the bond length distributions. However for Fe−pyridine species the occurrence of high- and low-spin states is immediately evident from the Fe−N bond length distributions. Figure 9 shows the distribution of Fe−N bond lengths for pyridines and substituted pyridines as defined in Figure 2.

The search fragment definition implies that only substituents bonded to the NC_5 ring by acyclic bonds are allowed; this meant that only simple, 'innocent' substituents which would be expected to have little chemical influence on the pyridine ring were included. The overall SSD here is slightly larger than for Fe−Cl structures, and in both cases the bond length distributions are bimodal. However, for the Fe−pyridine case the distribution remains clearly bimodal after the distribution has been subdivided on oxidation state and metal coordination number. The presence of low- and high-spin species is quite evident. The mean Fe−N bond length is significantly shorter for the low-spin cases. The difference in the mean Fe(II)−N bond lengths for high- versus low-spin cases is 0.19 Å (Table 5), in agreement with Gutlich,[30] and the difference for Fe(III) is similar at 0.16 Å. In the 1989 Dalton tables[1a] there were only 14 Fe−pyridine observations (cf. 139 in the present study), and so no division of the Fe−N bond lengths by spin state was made.

As noted above, it is not possible to search for high- or low-spin state in the CSD (except within the text data which are incomplete and unreliable). However, the bond valence sums which are used by the OXQUEST program to calculate the oxidation state of metals (vide supra) are themselves spin dependent, as the individual bond valence expression (S_{ij}) includes the M−L bond lengths, which (as shown for Fe−N) are sensitive to spin state. Both OXQUEST[11] and See et al.[7] consider only high-spin data in their calculation of BVS, as different R_o values would be required for low-spin structures. Therefore, if the oxidation state can be safely determined by the ligand template matching process, the BVS can be used to identify likely spin states. Figure 10 shows the Fe−N bond lengths plotted against BVS values for the 6-coordinate Fe(II)−pyridine data set. There is clear differentiation in BVS values for high- and low-spin cases (where identified as such in the primary literature). The BVS values are close to the formal oxidation state of Fe for the high-spin structures (as R_o values are based on data for high-spin species). The BVS values are much higher for the low-spin structures. Therefore, BVS values do not correctly predict oxidation state for low-spin complexes (see Table 6).

The use of BVS to analyze spin state is successful for a range of Fe−pyridine derivatives including 2,2′-bipyridine (bipy) and *o*-phenanthroline (phen), as shown in Table 6. Similar performance is seen for Co−bipy fragments (Table 6). In this case, the Co(II)−bipy bond length distribution has 2 short Co−N bond lengths (2.012 Å, 2.014 Å) for which the BVS value is high. This indicates, correctly, that these

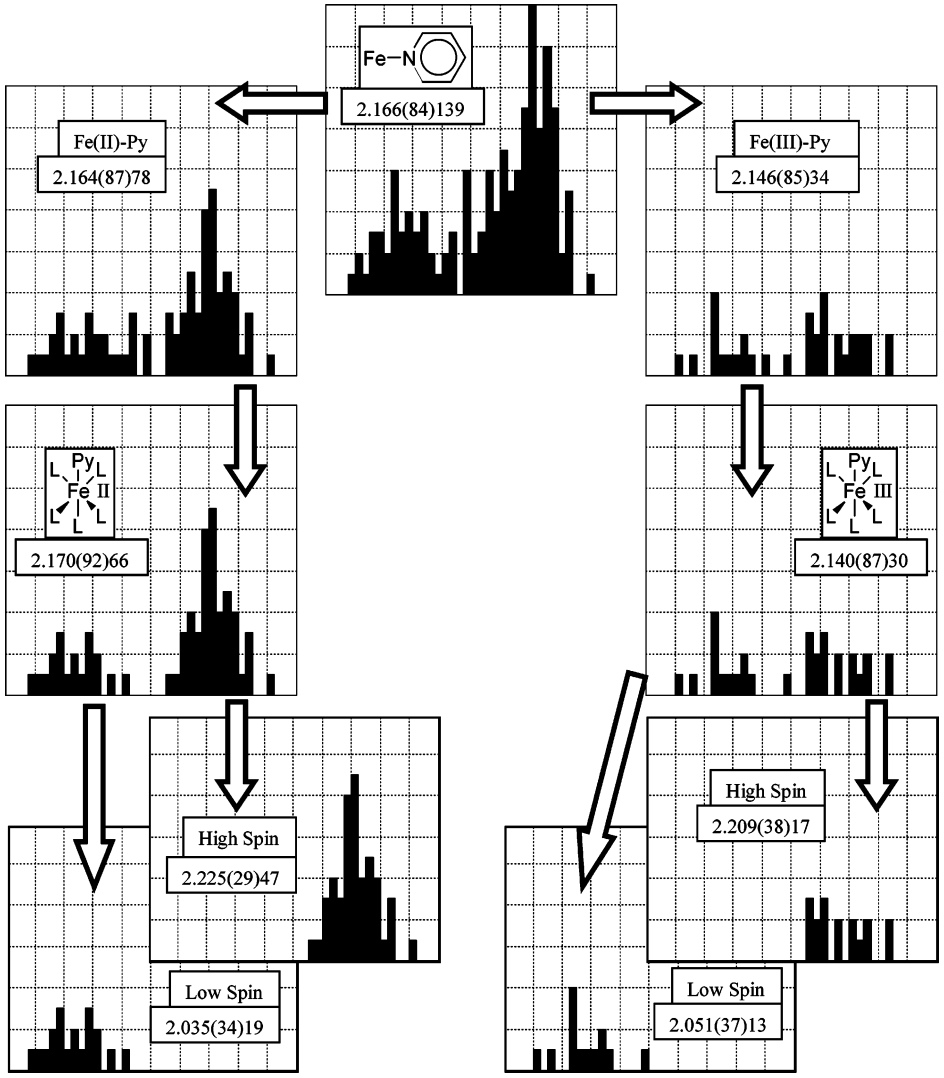

Figure 9. Histograms of Fe−N bond lengths upon division by oxidation state, metal coordination number, and spin state.

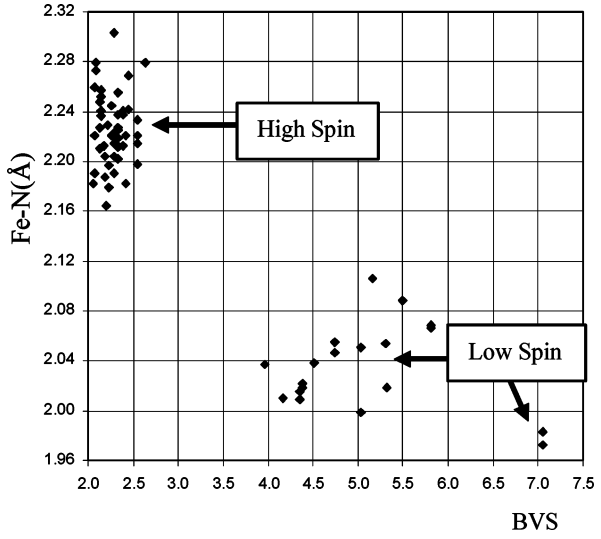

Figure 10. Correlation between Fe−N bond lengths and calculated BVS values for 6-coordinate Fe(II)−pyridine fragments showing low- and high-spin groups.

bond lengths belong to a low-spin structure.[31] Manganese(III) complexes can be either high or low spin and also show Jahn−Teller effects (for high-spin structures). As discussed above, the Mn−Cl bond length distribution for 6-coordinate Mn(III)−Cl species is bimodal, apparently as a consequence of Jahn−Teller effects. Table 6 shows that the BVS values correctly predict the oxidation state for all Mn(II)−Cl and Mn(III)−Cl structures, indicating that they are all high spin. Even those fragments with long Mn−Cl bond lengths do not give BVS substantially different from 3.0. Therefore, at least in this case, BVS values can successfully distinguish between spin and Jahn−Teller effects.

Tertiary Phosphines. Tertiary phosphine and other soft ligands form complexes with higher metal−ligand covalency.[32] We therefore chose to inspect bond length distributions for this type of structure, using the same (or similar) criteria as for the more classical coordination complexes analyzed above. For these structures, the BVS method for calculating oxidation state proved generally unreliable, typically producing unrealistically high values. Therefore, oxidation states were in most cases assigned solely by ligand template matching and sometimes by hand.

The Ni−P bond length distribution for triarylphosphines, PAr_3, as defined in Figure 2 (most of the fragments are from PPh_3 complexes) has a SSD (0.06 Å) and distribution (see Figure 11) similar to many of the coordination complex fragments discussed above. There are two Ni−P bond lengths (2.455 Å and 2.552 Å) more than 4σ from the mean (2.203 (60) Å). These are both for 6-coordinate Ni(II) structures

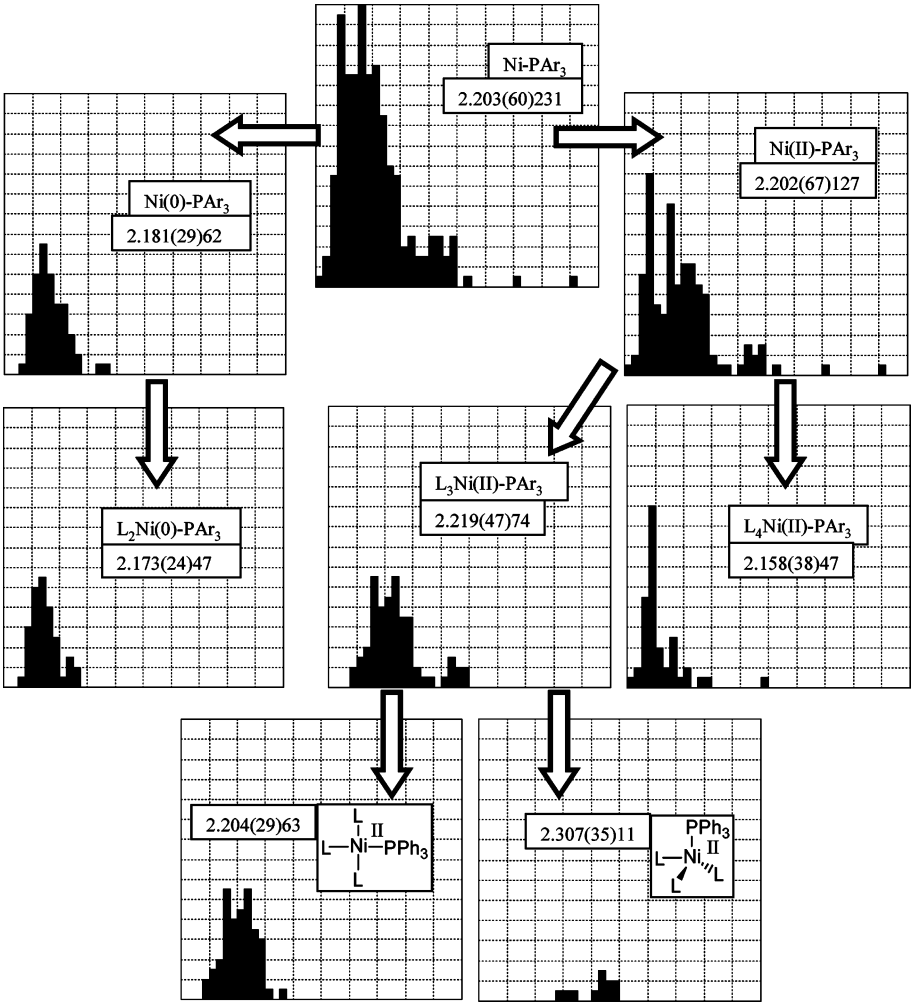

Figure 11. Histograms of 231 Ni−PAr_3 bond lengths upon division by oxidation state, metal coordination number, and nickel coordination geometry.

Table 4. Mean Cu−OH_2 Bond Lengths (Å) for Terminally Bonded H_2O

total fragments	oxidation state	metal coordn no. (geometry)	trans ligand	Jahn−Teller effect
2.223 (224) 1642	Cu(I): 2.288 (34) 10			
	Cu(II): 2.222 (225) 1616	4: 1.962 (31) 27	N: 1.949 (24) 12	
		all square planar		
		5: 2.211 (187) 801	N: 1.967 (29) 133	
			O: 1.966 (28) 65	
			no trans ligand[a]	Cu−O < 2.1 Å: 2.037 (48) 18
			2.310 (121) 522	Cu−O > 2.1 Å: 2.320 (111) 504
		6: 2.245 (254) 778	N: 2.021 (144) 119	Cu−O < 2.1 Å: 1.973 (29) 105
				Cu−O > 2.1 Å: 2.377 (162) 14
			O: 2.285 (257) 499	Cu−O < 2.1 Å: 1.968 (29) 175
				Cu−O > 2.1 Å: 2.457 (132) 324
			M: 2.158 (40) 41	

[a] 'No trans ligand' defined as no O−Cu−L angles greater than 150°.

Table 5. Mean Fe−Pyridine Bond Lengths (Å)

total fragments	oxidation state	metal coordn no.	low/high spin	trans ligand
2.166 (84) 139	Fe(II/III) trimers: 2.242 (15) 17			
	Fe(II): 2.164 (87) 78	5: 2.113 (32) 7		
		6: 2.170 (92) 66	low: 2.035 (34) 19	N: 2.027 (18) 12
			high: 2.225 (29) 47	N: 2.230 (28) 38
	Fe(III): 2.146 (85) 34	6: 2.140 (87) 30	low: 2.051 (37) 13	N: 2.039 (46) 7
			high: 2.209 (38) 17	N: 2.201 (24) 7

where there are only three 6-coordinate Ni−PAr_3 fragments in the entire data set. The Ni−PAr_3 data set was divided on oxidation state and metal coordination number as before (Figure 11 and Table 7) and, for 4-coordinate Ni(II), on metal coordination geometry. This showed that Ni−P bond lengths are significantly longer for tetrahedral Ni(II) complexes

Table 6. Mean Metal−Ligand Bond Lengths (Å) and Range of BVS for 6-Coordinate M−L Complexes

M−L	metal Ox^n state	BVS	spin state	mean M−L (Å)
Fe−py	II	2.0−2.6	high	2.225 (29) 47
	II	4.0−7.0	low	2.035 (34) 19
	III	2.5−3.4	high	2.209 (38) 17
	III	3.9−4.5	low	2.051 (37) 13
Fe−bipy	II	2.5	high	2.214
	II	4.4−6.0	low	1.974 (21) 35
	III	2.5−3.3	high	2.163 (26) 47
	III	4.5−5.0	low	1.968 (13) 10
Fe−phen	II	2.3−2.75	high	2.205 (25) 7
	II	4.2−5.7	low	1.977 (23) 34
	III	2.8−3.2	high	2.205 (60) 36
Co−bipy	II	1.9−2.12	high	2.134 (24) 52
	II	2.72	low	2.012, 2.014
	III	2.7−3.6	high	1.943 (21) 36
Mn−Cl	II	1.84−2.2	high	2.494 (49) 71
	III	3.16−3.5	high	2.352 (131) 31

(which are high spin) than for square planar Ni(II) species (which are low spin). For the 5-coordinate Ni(II)−PAr_3 subset there is one Ni−P distance (2.340 Å) more than 4σ from the mean (2.158 (38) Å). All the 5-coordinate Ni(II) complexes are likely to be low spin. The long Ni−P bonds are all in apical tetragonal pyramidal sites. The other 5-coordinate Ni−PAr_3 bond distances are nonapical, and all but three are in η^5-Cp ligand or derivative complexes (see Table 7).

Metal−phosphine bond lengths were also studied (Table 7) for Mo−PC_3 and Re−PC_3 fragments [PC_3 = any tertiary phosphine with acyclic P−C bonds (Figure 2)]. It is known that M−P bond lengths are influenced by the nature of the phosphorus substituents due to the PA_3 π-acceptor orbital having P−A σ* character.[33] However, the difference in the influence of alkyl versus aryl on M−P bond lengths is generally relatively small and depends also on the nature of the alkyl group (e.g. ^{t}Bu compared to Me). Because of the variety of oxidation states and metal coordination numbers for Mo and Re phosphine fragments, all acyclic M−PR_3 and M−PAr_3 phosphines (including mixed R/Ar phosphines) were considered together, and a final division on the R/Ar group was made only if the number of structures allowed. As for some of the carboxylate and chloride systems above, division by the trans ligand gives the most substantial reduction in SSDs in this case. For example, the mean M−P bond length is longer when trans to another P ligand than an η^5-cyclopentadienyl ligand. However, in contrast to the harder ligands considered above, the mean M−P bond lengths generally do not increase with increasing coordination number, but in most cases decrease, and the SSDs often remain reasonably high after division on coordination number. For 6-coordinate Mo(0) with P trans to CO the phosphine ligands were divided on the phosphine substituents. The Mo−P bond lengths for P $(CH_3)_3$ or P $(CH_2R)_3$ are marginally shorter than for PAr_3 (although not significantly so in a statistical sense). Six-coordinate Re(V) species show the same behavior. As for Ni, there are a few M−P bond lengths more than 4σ from the mean for Mo and Re. For Mo, two long Mo−P bond lengths are from a Mo(II) 6-coordinate structure with the phosphine ligand trans to a Mo−Mo bond, and for Re the Re−P outliers are part of a 'metal cluster' structure.

Alkenes. Rhodium−η^2-alkene complexes were analyzed for alkenes of the form C(HC_α)=C(HC_α) (Table 8). The alkene fragment was defined so that the C_α groups were not bonded directly to Rh, and thus larger delocalized π-bonded systems were excluded (see Figure 2). A large number of the fragments (65%) were from cycloocta-1,5-diene complexes. Both individual Rh−C bond lengths in the Rh−alkene fragment were included in the data set. In most cases, the two distances are very similar. The Rh−C histogram is unimodal, and the SSD of 0.056 Å is similar to those for other fragments. Most of the fragments are Rh(I) species, and, as for the phosphine ligands, there is little reduction in SSD or variation in mean Rh−C bond on division by metal coordination number. However, as for other examples, dividing the bond lengths on the ligand trans to the alkene ligand gives smaller, reasonable SSDs. A final subdivision including only cycloocta-1,5-diene fragments has little effect on mean and SSD values.

METALLO-ORGANIC MOLECULAR GEOMETRY LIBRARY DEVELOPMENT

The overall objective of this work is to develop a procedure that will produce a molecular geometry library of M−L bond lengths (and in principle other descriptors) automatically, using all the metal−ligand bond geometry data stored in the CSD. This would then allow rapid and easy retrieval of chemically coherent structural data for a user-specified query or structure.

The examples detailed above have shown how, for a particular ligand or ligand group, dividing the data on some or all of the metal-based criteria [oxidation state, metal coordination number, metal coordination geometry, spin state, Jahn−Teller effect, and trans ligand] and ligand-based criteria [coordination mode and, in some instances, more specific ligand definition] typically gives unimodal data sets with SSDs of less than 0.04 Å and, in many examples, about 0.02 Å. On the basis of this experience, we now suggest an algorithm which would automatically compile a library of metal−ligand distances. We can envisage ideal behavior in which the molecular geometry library has a treelike structure dividing M−L data sets into increasingly more sharply defined distributions (with smaller SSDs), as instructed by the algorithm (Figure 12). Ideally, each further subdivision better defines the chemical nature of the M−L bond, in a manner similar to that shown in Figures 4, 5, 8, 9, and 11. Therefore, the final 'bins' should contain molecular fragments which are chemically similar and provide a mean bond length and SSD of value to, for example, molecular modelers, crystallographers and other structural scientists.

Construction of Molecular Geometry Library. The building of such a geometry library from the CSD can be envisaged as having 3 main steps:

1. CSD Data Adjustment:

• Standardization of metal−ligand connections. This is likely to be significant only for metals that show a particularly large range of M−L distances (and so inconsistent connectivity assignment). This is so for Cu, Ag, Zn, Cd, Hg, Tl, Ge, Sn, Pb, Sb, and Bi with oxygen, halogen, and nitrogen ligands.

• Standardization of metal−metal connections. Assignment of metal−metal bonds is not consistent in the CSD. M−M distances shorter than an appropriate cutoff should be classified as M−M bonds with cutoff varying according to

Table 7. Mean Ni, Mo, and Re−P Bond Lengths (Å) for Monodentate Tertiary Phosphines

M−P	total fragments	oxidation state	metal coordn. no.	metal coordn geometry	trans ligand	PC_3 groups
$NiPAr_3$	2.203 (60) 231	metal clusters: 2.209 (46) 20				
		Ni(0): 2.181 (29) 62	3: 2.173 (24) 47			
			4: 2.211 (31) 13	all tetrahedral		
		Ni(I): 2.268 (60) 18	3: 2.220 (25) 5			
			4: 2.307 (11) 10	all tetrahedral		
		Ni(II): 2.202 (67) 127	4: 2.219 (47) 74	tetrahedral: 2.307 (35) 11 square planar: 2.204 (29) 63		
			5: 2.158 (38) 47		η^5/η^6-C ligands: 2.149 (20) 43	
$MoPC_3$	2.519 (63) 649	metal clusters: 2.579 (39) 52				
		Mo(0): 2.524 (49) 125	6: 2.524 (49) 124		carbonyl: 2.550 (29) 80	C = CH_3, CH_2R only: 2.544 (23) 7 PAr_3: 2.565 (23) 17
					η^5/η^6-C ligands: 2.446 (19) 15	
					P: 2.492 (18) 23	
		Mo(I): 2.473 (65) 29	6: 2.523 (53) 15			
			7: 2.420 (14) 14			
		Mo(II): 2.499 (70) 229	5: 2.539 (25) 63		P: 2.542 (26) 46	
			6: 2.491 (92) 85		η^5/η^6-C ligands: 2.434 (25) 11	
					P: 2.504 (43) 43	
			7: 2.476 (51) 80		η^5/η^6-C ligands: 2.470 (32) 44	
		Mo(III): 2.540 (43) 86	5: 2.565 (41) 5			
			6: 2.550 (37) 61		halogen: 2.542 (26) 32	
					P: 2.563 (29) 21	
			7: 2.502 (38) 20		η^5/η^6-C ligands: 2.512 (24) 18	
		Mo(IV): 2.511 (50) 99	5: 2.548 (37) 6			
			6: 2.521 (35) 42		P: 2.535 (23) 27	
			7: 2.512 (57) 27			
			8: 2.493 (53) 19			
		Mo(V): 2.567 (57) 19	6: 2.553 (24) 16			
$RePC_3$	2.434 (57) 1070	metal clusters: 2.476 (70) 104	ReM_5 clusters: 2.480 (12) 66			
		Re(0): 2.382 (34) 13	6: 2.369 (28) 10			
		Re(I): 2.429 (56) 172	6: 2.428 (56) 165		carbonyl: 2.484 (25) 61	
					η^5/η^6-C ligands: 2.332 (19) 12	
					P: 2.408 (28) 66	
		Re(II): 2.427 (44) 50	5: 2.428 (29) 28		P: 2.440 (25) 19	
			6: 2.442 (48) 18		P: 2.453 (41) 7	
		Re(III): 2.407 (51) 309	5: 2.427 (40) 21			
			6: 2.420 (46) 204		η^5/η^6-C ligands: 2.383 (29) 88	
					halogen: 2.417 (46) 13	
					N: 2.420 (20) 15	
					P: 2.464 (23) 76	
			7:2.374 (49) 83		η^5/η^6-C ligands: 2.357 (51) 31	
					H: 2.379(29)11	
		Re(IV): 2.467 (60) 71	6: 2.486 (36) 61		P: 2.496 (28) 33	
			8: 2.331 (15) 8			
		Re(V): 2.452 (42) 300	5: 2.440 (30) 26			
			6: 2.461 (36) 236		P: 2.481 (31) 106	C = CH_3, CH_2R only: 2.440 (24) 7 PAr_3: 2.491 (41) 39
					halogen: 2.449 (27) 56	
					N: 2.447 (21) 27	
					S: 2.426 (31) 22	
			8: 2.402 (51) 33 1>4σ, removed: 2.396 (36) 32			
		Re(VII): 2.432 (27) 22	9: 2.425 (22) 19			

Table 8. Mean Rh−C Bond Lengths (Å) for η^2-Alkene Ligands, C(HC)═C(HC)

total fragments	oxidation state	metal coordn no. (geometry)	trans ligand X−M−L² > 150°[a]	cycloocta-1,5-diene fragments only
2.149 (56) 1756	metal clusters: 2.187 (48) 74			
	Rh(I): 2.146 (52) 1647	4: 2.143 (51) 1204 all square planar	σ-C: 2.179 (31) 38	all cycloocta-1,5-diene fragments
			halogen: 2.104 (16) 138	2.105 (15) 104
			N: 2.127 (18) 315	2.128 (17) 241
			O: 2.100 (20) 266	2.099 (19) 208
			P: 2.226 (34) 229	2.237 (30) 157
			S: 2.145 (24) 149	2.148 (23) 129
		5: 2.153 (52) 435	η^5/η^6-C ligands: 2.130 (19) 186	2.130(20)76
			N: 2.145 (36) 70	2.149 (45) 28
			P: 2.245 (34) 41	2.244 (39) 13
			S: 2.206 (20) 10	2.206 (19) 8
		6: 2.164 (23) 8[b]		

[a] X = centroid of C═C bond. [b] Excluding 4 long Rh−C bonds (2.435−2.485 Å) with C═C bond trans to another Rh.

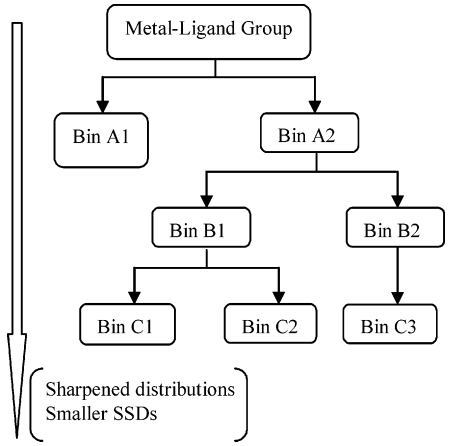

Figure 12. Treelike structure of molecular geometry library.

metal size. Ideally formal metal−metal bond order should be assigned, but this will require additional data to be stored in the CSD.

- Assignment of metal as part of a metal cluster if it is bonded to two or more metal atoms.
- Assignment of oxidation state for all metal atoms (see below).

Standardization of both M−L and M−M connectivity is important for correct identification of metal clusters, coordination number and geometry, BVS and trans ligand, etc.

2. Ligand classification:

To characterize the metal coordination environment and so allow classification of any individual M−L bond and analysis of its geometry, ligands must be accurately classified. For the organic version of this library (Mogul),[3] the chemical environment of a particular molecular fragment (bond, valence angle or torsion angle) is described by a set of keys which effectively defines a substructure centered on and extending two bonds out from the fragment. However, for the previous tabulation of metal−ligand geometry[1a] and the case studies reported here, the ligand grouping used for subdivision has been either

(I) an exact ligand, e.g. chloride or water, or

(II) a ligand class, e.g. carboxylates, tertiary phosphines, acyclic pyridines in a particular bonding mode.

The key method used for organic species would not give sufficient discrimination between the varied ligand types found in the CSD. In addition, for many ligands there are bond type inconsistencies in the CSD which give rise to added complications. Therefore, it seems that the best approach is to identify and classify according to a library of ligand templates as discussed below.

This ligand classification would involve the following:

- Assignment of every ligand, L, in the CSD to a template (or templates) as defined in a ligand template library (see below).
- Classification of ligands to "ligand classes" (e.g. tertiary phosphines, porphyrins, etc.) based (in part) on the contact atom of the ligand.
- Assignment of the binding mode of ligand, as, e.g., monodentate, chelating, bridging.

3. Subdivision algorithm:

For each metal−ligand bond classified according to the class of ligand and the binding mode, the bond geometry data distribution should be subdivided to give chemically coherent data sets according to metal-based criteria (metal oxidation state, coordination number, coordination geometry, spin state and Jahn−Teller effect and trans ligand). The resulting data sets may then be further subdivided according to finer classification of the ligand type, as defined in the ligand template library (see below).

Ligand Template Library. As noted above, for a geometry library to be constructed from all the metal−ligand bonds available in the CSD, all ligands in all metal-containing crystal structures must be identified and correctly classified. This implies assigning each ligand as matching a particular ligand template.

Here we define a ligand as any nonmetal atom, or group of covalently linked nonmetal atoms, bonded to a metal. The nonmetal elements are assumed to be H, B, C, N, O, F, Si, P, S, Cl, As, Se, Br, Te, and I. Two ligands are deemed to be the same if they have the same connectivity and stereochemistry (i.e. ligand charge is ignored).

A survey of the occurrence of such ligands showed there were approximately 780 000 present in the October 2001 version of CSD (which contained 250 760 structures). These corresponded to 22 000 unique ligand formulas. Only 70 formulas (for example CO, Cl, C_5H_5) had more than 1000 occurrences. These 70 formulas accounted for ca. 70% of all ligands. In contrast ca. 19 000 formulas occurred less than 10 times. We will report this survey and the development of the ligand template library fully elsewhere but outline its main features here for convenience.

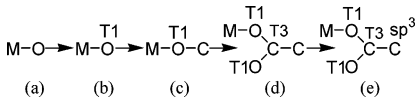

Figure 13. Family of generic ligand templates required to describe an alkyl carboxylate ligand (RCO_2). Tn values refer to the number of nonmetal atoms bound to a particular atom.

The strategy used for ligand classification is to create a ligand template library in three parts, as follows:

1. Exact ligand templates:

These define the exact structures of all the common ligands (e.g. having 100 occurrences and more in the CSD) and other ligands which are deemed chemically important, e.g. by virtue of their simplicity. All ligand atoms and their connectivity and stereochemistry are completely described. We have defined to date approximately 730 exact templates including the following: PPh_3; 2,2′-bipy; CO; Cl; N, etc.

2. Innocently substituted templates:

These are exact ligand templates with terminal hydrogen atoms replaced by 'innocent' substituents (alkyl etc.), where "innocent" substituents are assumed not to have a major effect on the M−L behavior of the ligand. For example the 'innocently substituted' permethylcyclopentadienyl group would include ethyltetramethylcyclopentadienyl.

3. Generic ligand templates:

These ligand templates cover all other ligands in the CSD. To ensure that all ligands can be described by a ligand template, the ligands are first classified according to the contact atom bonded to the metal and the number of nonmetal atoms bound to the contact atom. Figure 13 shows how the family of oxygen templates can be subdivided to identify the carboxylate ligand class (step (d)) and can be further subdivided, for example, on the hybridization of the substituent C atoms, to afford the alkyl carboxylates of ligand template (e). Finally, templates (e) could be refined to afford exact templates, e.g. acetate, propionate, etc.

This ligand template library has a treelike structure, with the templates becoming more chemically and structurally specific as one descends the tree. The exact ligand templates would be placed at the end of a particular branch, with the innocently substituted ligand templates usually one level less specific. The "ligand class" to which a given ligand would belong therefore corresponds to one of the earlier subdivisions of the generic ligand classification (such as stage (d) in Figure 13). This subject is discussed in more detail in the section on generalization below. The structure of the ligand template library thus resembles that of the molecular geometry library itself (Figure 12).

Binding Mode. As noted above, assignment of both the ligand and its binding mode are required in order to characterize the metal coordination environment fully. Complex multidentate ligands may then be described as being composed of a combination of a number of generic ligands fused together. This is not without complexity for polychelating ligands.

Subdivision Algorithm. A proposed algorithm for subdividing the M−L geometry data for a given ligand class is shown in Figure 14. The criteria (and sequence) used for subdivision of a given distribution are based on those employed in the M−L case studies analyzed above. Therefore, for a given metal−ligand combination the distribution of geometry data is divided on metal-based criteria (metal

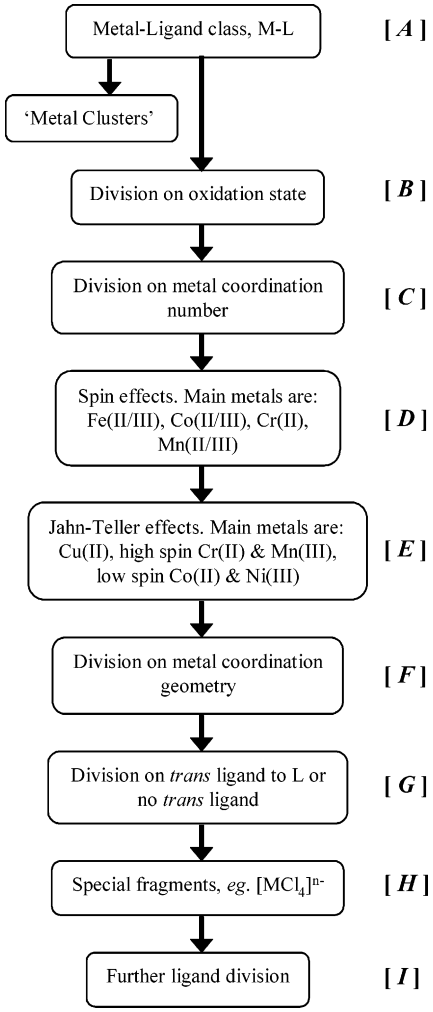

Figure 14. General algorithm for M−L bond length analysis.

oxidation state; followed by metal coordination number, spin and Jahn−Teller effects, metal coordination geometry and trans ligand and special, common structure types) and then on finer classification of the ligand group. In automatic compilation of M−L data sets not all steps are likely to be required for all metal−ligand fragments. Below we consider how this algorithm might be applied to CSD data to produce a useful molecular geometry library for metallo-organics, to supplement the library already produced for organic structures.[3]

The steps to be completed in the algorithm are listed in sequence A to H below.

Step A. In this first step, the metal−ligand (i.e. ligand class and binding mode) combination is identified. Metal cluster structures, as assigned by M−M connectivity, are then removed from the data set and dealt with separately.

Step B*:* Oxidation State. The OXQUEST program, as discussed in the Methods and Procedures section above, calculates individual oxidation states by 2 methods (BVS and ligand template matching), the oxidation state being accepted if the methods agree. These calculations may be in error for structures with missing ligands (e.g. hydride or disordered species), and so these cases must be removed from the data sets or dealt with separately.

To investigate the ability of OXQUEST to assign metal oxidation states, data sets of M−Cl fragments that are not part of a metal cluster were analyzed for all *d*-block metals.

The percentage of M-Cl fragments where the oxidation state of M calculated by the 2 methods agrees to within half a unit was calculated for each metal.

Best agreement (85% or greater) between the two methods was found for the first row *d*-block metals of Mn, Fe, Co, Cu and Zn and La, Cd and Hg. Agreement was worst, with less than 50%, for Ti and the third and second row transition metals of groups 4 to 9 inclusive (i.e. Zr, Nb, Mo, Tc, Ru, Rh, Hf, Ta, W, Re, Os, Ir). Failure of the two methods to agree was either due to a given ligand not matching an available ligand template or, more often, the ligand template method giving the correct oxidation state and the BVS value being in error. BVS usually gives erroneous oxidation state values for structures with soft ligands and for low-spin structures (vide supra). For the cases where the ligand template method failed, the oxidation state was assigned by hand. The observation that BVS outcome depends on ligand type (as well as metal type), but is largely independent of metal coordination number and geometry, is in general agreement with observations by See and co-workers.[7]

Therefore, it seems reasonable that the ligand template method should be used as the sole means of oxidation-state assignment for many metals. While the current OXQUEST software occasionally fails through lack of a suitable ligand template, extension of the ligand template library (see above) should alleviate this problem.

Finally, it is noteworthy that the assignment of oxidation state (and other characteristics, see below) only needs to be done once and can then be stored for all future geometry libraries, given suitable CSD database architectures.

Step C*:* Metal (Effective) Coordination Number. As for oxidation state, this criterion was used in all metal−ligand case studies discussed above. OXQUEST routinely calculates coordination numbers for all metals, as noted above it may be in error for structures with missing (hydride or disordered) ligands, and so these cases must be removed from the data sets or dealt with separately.

Step D*:* Spin Effects. This criterion only needs to be included in the algorithm for particular metals, as discussed above and shown in Figure 14. For other metals, spin affected cases should be clear outliers. Recognizing and identifying the spin state for the metals concerned can be difficult, and, as shown in the examples above, only one spin state may be present for some ligand groups. For example, Co−carboxylates and Fe−Cl fragments (except for a few 5-coordinate Fe(III)−Cl complexes) all appear to be high spin. For Mn(III), Cr(II), and Co(II) species, there is the added complication of Jahn−Teller effects (see step E below).

For 4-coordinate complexes, different spin states will be associated with different metal geometries. Tetrahedral species are typically high spin and square planar are low spin (see step F below). Therefore, spin effects (and subdivisions made on these criteria) are best assessed after oxidation state and metal coordination number have been established. Given the difficulties in assigning spin states, as shown in the 5-coordinate Fe(III)−Cl data set, the geometry library might sensibly indicate to users that there may be spin effects in a given M−L data set. This may be manifested through the presence of outliers or bimodal or broad distributions leading to high SSDs (typically > 0.07 Å). If there is a clearly bimodal distribution, it might be divided into two groups either automatically or by the user. For example, in the Fe−pyridine example, the low-spin cases would be identified as the group with shorter M−L bond lengths. Conversely, if by this stage in the algorithm (after division by oxidation state and metal coordination number) the data set is unimodal with no outliers and a reasonable SSD (<0.04 Å), the program could flag that all structures appear to be of one spin type, and, depending on the ligand, it may be possible for the program to identify the correct spin state using the BVS method.

Step E*:* Jahn−Teller Effect. As for spin effects, Jahn−Teller effects only occur for certain metals in particular oxidation states (and spin states) and only applies significantly to 5- and 6-coordinate metal complexes (see Figure 14). Therefore, this step should also be applied after division on oxidation state and metal coordination number. Jahn−Teller effects should be evident by the presence of outliers or a broad distribution and thus high SSD (>0.07 Å) and, in some cases, a bimodal distribution.

Step F*:* Metal Coordination Geometry. In the case studies reported here, only the 4-coordinate geometries were subdivided by coordination geometries (apart from 5-coordinate Mn(III)−Cl fragments, where the tbp and tetragonal pyramidal geometries were easily assigned). In developing the geometry library, division on 4-coordinate geometries could be considered initially. Various methods to define 5- and higher coordinate geometries have been reported (see above), and subdivisions of these data sets could be considered as a further development. For 5-coordinate species, subdivision on trans ligand will divide the M−L bond lengths into whether there is a ligand trans to M−L bond length or not (see step G below) and therefore identify apical tetragonal pyramidal and equatorial tbp ligands.

For 4-coordinate structures, the geometry is relatively easy to define. For certain metals (e.g. d^8 Ni(II)), the coordination geometry for a particular oxidation state is indicative of low (square planar) or high (tetrahedral) spin state which in turn affects the M−L bond lengths (see above, Ni−PAr_3). However, for many 4-coordinate metal−ligand data sets, only one metal geometry is present.

Table 9 shows the distribution of tetrahedral (all L−M−L ≤ 140°), square planar (L^1−M−L^2, L^3−M−L^4 ≥ 150°), disphenoidal (L^1−M−L^2 ≥ 150°, L^3−M−L^4 ≤ 130°), and the severely distorted structures which are not defined by one of these 3 geometries, for all 4-coordinate complexes other than clusters. Table 9 shows that there are a number of metals on the left of the transition series which almost always adopt tetrahedral geometry. In groups 9 and 10 Rh, Ir, Pd, and Pt have structures in all 3 possible geometries with some significantly distorted examples, but the majority are square planar (and have d^8 electron configuration). In groups 11 and 12 and the first row metals from Cr to Ni the largest variation is seen. This is in general agreement with the conclusions of Alvarez et al. in their detailed database study of 4-coordinate geometries.[21] We will return to the issue of how to deal with "unusual" geometries in a fairly automatic manner in a subsequent paper.

The analysis of Table 9 shows that, for some metals, division on coordination geometry need not be included in the algorithm as all known examples are of the same type (e.g. for the metals of groups 3 and 4). If oxidation state is taken into account, as analyzed by Alvarez,[21] there would be even less variation (e.g. for Rh and Ir). Alvarez showed

Table 9. Coordination Geometries of 4-Coordinate Metal Complexes in the CSD (Nov 2003)[a]

3	4	5	6	7	8	9	10	11	12
Sc	Ti	V	Cr	Mn	Fe	Co	Ni	Cu	Zn
Td	Td	T sq ds	T SQ ds d	T sq ds d	T SQ ds D	T SQ DS D	SQ T ds D	T SQ DS D	T SQ DS D
Y	Zr	Nb	Mo	Tc	Ru	Rh	Pd	Ag	Cd
T	Td	Td	Td	T	T sq ds d	SQ T ds D	SQ T ds d	T SQ DS D	T SQ ds D
La	Hf	Ta	W	Re	Os	Ir	Pt	Au	Hg
T	T	T	T sq	T sq	T sq d	SQ T ds d	SQ T ds D	SQ T DS D	T SQ DS D

[a] Definitions of the 3 geometries are given in the text. [T: tetrahedral; SQ (sq): square planar; DS (ds): disphenoidal; D (d): distorted structures.] T, SQ, DS, and D specify more than 10 fragments for a given metal with defined coordination geometry, sq, ds, and d less than 10 fragments with specified geometry.

Table 10. Trans Ligands in Various Metal Coordination Geometries

metal coordn no.	metal coordn geometry	ligand trans to M−L bond	no ligand trans to M−L bond
4	tetrahedral	no	yes
	square planar	yes	no
	disphenoidal, M−L axial	yes	no
	disphenoidal, M−L equatorial	no	yes
5	Tbp, M−L axial	yes	no
	Tbp, M−L equatorial	no	yes
	tetragonal pyramidal, M−L apical	no	yes
	tetragonal pyramidal, M−L equatorial	yes	no
6	octahedral	yes	no

Table 11. Subdivision Criteria, as Defined in Figure 14, Used for Each of the Metal−Ligand Examples Reported

metal−ligand group	division criteria
Co/Rh/Pt-carboxylate	B C G
Fe−Cl	B C G H
Hg−Cl	B C F G H
Mn−Cl	B C E F G H
Pd−Cl	B C G H
$Cu-OH_2$	B C G E
Fe−pyridine	B C D G
$Ni-PAr_3$	B C F G
Mo−PC_3 and Re−PC_3	B C G I
Rh-[η^2-C(HC)═C(HC)]	B C G I

that, for example, metals in d^0, d^1, d^2 electron configurations are almost all tetrahedral, while for d^8 and d^9 most are square planar. However, even if no division is required, it may be useful for the metal coordination geometry to be known and given to the user. It would also be of interest to know if there is more than one metal geometry present in the data set. This information might lead to identification of erroneous structural data, misassigned oxidation state, or characterization of an unusual ligand effect.

Step G: Trans Ligand. The ligand trans to the M−L bond is an important factor in the case studies above and, in the general algorithm, is the last main metal-based criterion. Whether there is a trans ligand will depend on the metal coordination geometry, as shown in Table 10. This division should be relatively easy to automate. In the automated system, trans ligands could be differentiated to distinguish between, for example, oxo and other O ligands (in the present study, in general, only the contact atom type was considered, see above). However, if the trans ligand is too specific, the number of fragments in the data sets will become too small.

Step H*:* Special Fragments. This division would be used in generating data sets for particular complexes (or families of complexes), where there is a substantial number of examples of a very tightly defined sort (e.g. $[MCl_4]^{n-}$, $M_2(\mu\text{-}O_2CR)_4$, or $[M(OH_2)_6]^{n+}$ etc).

Step I*:* Ligand Specification. Where there are sufficient data, the geometry distribution would be further subdivided according to finer classification of the ligand—initially using the generic ligand templates, the innocently substituted, and finally the exact level of ligand specification. This is discussed further below in terms of generalization.

Tailored Algorithms. So far, we have considered the criteria for subdivision of metal environment in a set sequence. To optimize efficiency when used in practice, the sequence might be varied. As noted above, spin and Jahn−Teller effects must of necessity be assessed after oxidation state and metal coordination number have been assigned, and it is obvious that division on coordination geometry must follow division on coordination number. However, other criteria might be applied in different sequence or not applied at all. For example, it may be unnecessary to subdivide on oxidation state or metal coordination number in all cases.

In Table 11, the sequence of criteria used for the particular case studies is reviewed in this light. While oxidation state, coordination number, and trans ligand were used in all these case studies, coordination geometry and spin and Jahn−Teller effects were only significant for some. The optimal order of the criteria for division of the data sets is essentially the same as that given in Figure 14, except for $Cu-OH_2$, where the division into short and long (Jahn−Teller affected) bonds was carried out after the trans ligand subdivision.

In the automated generation of the molecular library, tailored algorithms could be used to exploit knowledge of, e.g. whether the metal can or cannot exhibit varied oxidation state, etc. For example, the algorithm for metals Zn and Cd would be only coordination number, metal coordination geometry, trans influence, and common fragments, as all Zn/Cd complexes would be +2 oxidation state with no spin or Jahn−Teller effects.

Such an approach could be refined further if the algorithm were more data-driven. In such an approach, statistical criteria might be defined to produce the maximum reduction in SSD at each level of the data tree and to eliminate some levels of the tree altogether for particular M−L data sets. For example, in some M−Cl data sets the 4-coordinate fragments are all of one geometry (e.g. W, Re). Similarly division by trans ligand has been included for all metals, but in some instances cis influence is known to be of similar importance to trans influence.[34] Data-driven algorithms are considered in more detail below, after further developing the context in which they might be used.

Generalization. When the number of M−L fragments in the final data set is small or zero, it is necessary to "generalize" the search by using data from related fragments.

This means moving back to a higher, less specific level of the data tree (see Figure 12), where there should be a larger number of less chemically specific M−L fragments. The occasional necessity for this type of generalization makes the order of the division criteria in the algorithm important, since it is desirable to generalize the least significant features first.

As shown in Figure 14, the first step (A) in classifying M−L fragments is to assign the ligand to a general type, e.g. carboxylates. After subdivision on a range of metal properties, the last step (I) of our algorithm is a finer ligand classification, e.g. C (sp3)-bound carboxylate or—even more specific—acetate. Both at steps A and I, one would ideally want to use as specific a ligand classification as possible, so that the algorithm obtains the most chemically coherent M−L data sets. However, this needs to be offset against the need for sufficient data. If the ligand group is too specific, the number of data will be too small.

For the nickel tertiary phosphine examples reported above, the metal-property subdivision algorithm was applied to the relatively chemically specific PAr_3 phosphine ligand group. For Rh and Mo, the ligand group was defined as PC_3, where C is any carbon, and subdivision to more specific phosphines was applied after metal-property subdivision when there were sufficient data (Table 7). The PC_3 ligand group gave data sets with reasonable characteristics (number of fragments, means, and SSDs) in most cases. For many of the Rh and Mo data sets, a more specific ligand group would give too small a number of data. For the Co and Rh carboxylate examples, the analysis was carried out with rather specific carboxylate ligand classes, e.g. alkyl carboxylates. For Pt, a more generic carboxylate ligand group, O_2CC, was used with apparently little adverse effect on the statistics obtained (Table 2). Again, the final Pt−carboxylate data sets could have been divided to more specific ligand groups (e.g. alkyl carboxylates) after subdivision on metal properties. For the Rh−alkene data set, the final subdivision was to yield data only for the "exact" ligand cycloocta-1,5-diene (Table 8).

In these examples, the less specific ligand groupings at step A perform well, and this might tempt us to use even more general ligand classifications, so that the data set sizes at the metal-property subdivision stage are larger. Taking the carboxylate example in Figure 13, the subdivision algorithm was performed on the carboxylate ligand class (d). However, the even less specific ligand group (c) might be used, and the division into ligand classes be the final step (I) of the algorithm. The danger with this approach is that it might give overly general M−L data sets, and thereby make it more difficult to classify spin and oxidation states and identify outliers. In summary, the optimum specificity of ligand classification at step A will depend on the amount of data available but should aim to give the largest data sets which are chemically coherent. In extreme cases, e.g. Eu−P bonds, there are so few data (12 examples in this case) that no subdivision by ligand type will be possible at all, either at step A or I.

The algorithm put forward in this paper is chemically driven; however, one could instead construct an algorithm which is purely data driven. If the algorithm were completely data driven, the first division of the data set for a given metal−ligand group should be that which gives the biggest reduction in SSDs, preferably with a reasonably equal number of fragments in each subdivided group. Conversely, the final division of M−L data sets should lead to the smallest reduction in SSDs. Then, if and when generalization is needed, the final subdivision will be removed first. A data driven algorithm is likely to be different from a chemically intuitive algorithm. Below, we review the two options by reference to the bond length case studies in this paper.

Considering the metal-based criteria for both monodentate and bridging Co−carboxylate fragments (Table 2), oxidation state is arguably the most important criterion. However, for Fe−Cl fragments the SSDs remain high for both Fe(II) and Fe(III), although there is some difference in the mean Fe−Cl bond lengths (Table 3). For $Cu-OH_2$ fragments, almost all of the 1642 fragments are Cu(II) with only 10 Cu(I) cases. Also, for the softer ligands, e.g. tertiary phosphines, it is not obvious that oxidation state gives the biggest reduction in SSDs for the data set. In general terms, it could be argued that, for soft base−soft metal complexes, oxidation state is not as important as for coordination complexes (hard acid−base), and thus oxidation state should not be the first criterion in these cases. Similarly in coordination complexes coordination number is generally a more important factor than it is for organometallics. Test studies of algorithms with permuted sequences of subdivision on oxidation state, metal coordination number, and trans ligand did not clearly indicate a "best" sequence, although it was evident that all three criteria are important. There does not seem to be an overwhelming case for tailored algorithms.

Furthermore it is likely to be impractical for the algorithm for a particular metal−ligand group to be completely data-driven, as different algorithms would be required for different metals and different ligands with different editions of the CSD. All alternative algorithms would have to be tried and the 'best algorithm' then assigned. Given these conclusions, and the practical difficulty of implementing a data-driven approach, at least initially it may be best to use a single algorithm with no variation in the order of the data tree criteria, while noting that some criteria are not required for particular metal−ligand groups as discussed above. Since this is a geometry library, likely to be most widely used in a chemical context, the most 'chemically intuitive' algorithm of Figure 14 may be the most appropriate and is therefore likely to be preferred in the first instance, in part because of its audience. After construction of the library and examination of the resulting data sets it may then be evident that different ligand classes or alternative algorithms would be more appropriate for certain systems, for example, in ligand groups which we have not yet analyzed. However, it should be borne in mind that algorithms which are particularly suited to bond length data may not yield optimal subdivisions for the bond angles or torsion angles involving that bond.

CONCLUSIONS AND SUMMARY

In summary, we have explored how one could produce a molecular geometry library from metal−ligand bond length data as stored in the CSD. It would be hoped that such a library would allow users to retrieve chemically useful, well-defined metal−ligand bond geometry information, more efficiently than is presently possible. The approach adopted has been to take hand-crafted case studies for a range of metals and ligands and examine the factors which influence

the metal−ligand bond length. It seems that a standard algorithm may be used for all the cases analyzed and would lead to chemically and statistically coherent data in most cases.

To construct the molecular geometry library we can envisage three main steps:

1. standardize the CSD bond data and assign metal oxidation state,

2. classify all ligands and their bonding modes in the CSD,

3. divide the metal−ligand data sets according to the standard algorithm to give unimodal data sets with reasonable SSDs.

The standard algorithm sequence of criteria used in step (3) for a specified metal−ligand (class) group involves successive subdivision on

i. oxidation state,

ii. metal coordination number,

iii. spin state,

iv. Jahn−Teller effect,

v. metal coordination geometry,

vi. trans ligand,

vii. common groups, followed by more specific ligand assignment.

This algorithm is chemically—rather than data-driven and gives reasonable data sets for all the examples reported. The case studies cover a considerable spectrum of coordination and organometallic chemistry, including 'difficult' areas such as mercury chloride chemistry.

Treatment of spin state and Jahn−Teller effects is a significant issue but is only required for certain metals and oxidation states. We have shown in the iron−pyridine system that it is possible to assign spin state using bond valence sum (BVS) values as calculated in the OXQUEST program.

Alternative subdivision sequences have been explored, particularly with reference to generalization. However, we conclude that the sequence of steps summarized in Figure 14 should be adequate for most, if not all, cases.

ACKNOWLEDGMENT

Dr. Greg Shields is thanked for advice and software contributions. The EPSRC is thanked for financial support (for S.E.H.).

Supporting Information Available: Lists of CSD reference codes and metal−ligand bond lengths for each metal−ligand data set defined in Table 1: Co−carboxylates (Table S1); Rh−carboxylates (Table S2); Pt−carboxylates (Table S3); Fe−Cl (Table S4); Hg−Cl (Table S5); Mn−Cl (Table S6); Pd−Cl (Table S7); Cu−OH_2 (Table S8); Fe−pyridine (Table S9); Ni−PAr_3 (Table S10); $MoPC_3$ (Table S11); $RePC_3$ (Table S12); and Rh−alkene fragments (Table S13). This material is available free of charge via the Internet at http://pubs.acs.org.

REFERENCES AND NOTES

(1) (a) Orpen, A. G.; Brammer, L.; Allen, F. H.; Kennard, O.; Watson, D. G.; Taylor, R. Tables of bond lengths determined by X-ray and neutron diffraction. Part 2. Organometallic compounds and coordination complexes of the d- and f-block metals. *J. Chem. Soc., Dalton Trans*. **1989**, S1−S83. (b) Allen, F. H.; Kennard, O.; Watson, D. G.; Brammer, L.; Orpen, A. G.; Taylor, R. Tables of bond lengths determined by X-ray and neutron diffraction. Part 1. Bond lengths in organic compounds. *J. Chem. Soc., Perkin Trans. 2* **1987**, S1−S19.

(2) Allen, F. H. The Cambridge Structural Database: a quarter of a million structures and rising. *Acta Crystallogr., Sect. B* **2002**, *58*, 380−388.

(3) Bruno, I. J.; Cole, J. C.; Kessler, M.; Luo, J.; Motherwell, W. D. S.; Purkis, L. H.; Smith, B. R.; Taylor, R.; Cooper, R. I.; Harris, S. E.; Orpen, A. G. Retrieval of crystallographically derived molecular geometry information. *J. Chem. Inf. Comput. Sci.* **2004**, *44*, 2133-2144.

(4) Harding, M. M. The geometry of metal−ligand interactions relevant to proteins. *Acta Crystallogr., Sect. D* **1999**, *55*, 1432−1443.

(5) Harding, M. M. The geometry of metal−ligand interactions relevant to proteins. II. Angles at the metal atom, additional weak metal-donor interactions. *Acta Crystallogr., Sect. D* **2000**, *56*, 857−867.

(6) (a) Harding, M. M. Geometry of metal−ligand interactions in proteins. *Acta Crystallogr., Sect. D* **2001**, *57*, 401−411. (b) Harding, M. M. Metal−ligand geometry relevant to proteins and in proteins: sodium and potassium. *Acta Crystallogr., Sect. D* **2002**, *58*, 872−874.

(7) See, R. F.; Kruse, R. A.; Strub, W. M. Metal−ligand bond distances in first-row transition metal coordination compounds: Coordination number, oxidation state and specific ligand effects. *Inorg. Chem.* **1998**, *37*, 5369−5375.

(8) Hocking, R. K.; Hambley, T. W. Structural measure of element-oxygen covalency from the changes to the delocalisation of the carboxylate ligand. *Dalton Trans*. **2005**, 969−978 and references therein.

(9) Martin, A.; Orpen, A. G. Structural systematics. 6. Apparent flexibility of metal complexes in crystals. *J. Am. Chem. Soc*. **1996**, *118*, 1464−1470.

(10) Orpen, A. G.; Quayle, M. J. Geometry variation of complex ions in crystals. *J. Chem. Soc., Dalton Trans*. **2001**, 1601−1610.

(11) Shields, G. P.; Raithby, P. R.; Allen, F. H.; Motherwell, W. D. S. The assignment and validation of metal oxidation states in the Cambridge Structural Database. *Acta Crystallogr., Sect. B* **2000**, *56*, 455−465.

(12) House, D. A.; Robinson, W. T.; McKee, V. Chloromercury(II) anions. *Coord. Chem. Rev*. **1994**, *136*, 533−586.

(13) Beckwith, J. D.; Tschinkl, M.; Picot, A.; Tsunoda, M.; Bachman, R.; Gabbai, F. P. Interaction of the bifunctional lewis acid 1,2-bis (chloromercurio) tetrafluorobenzene with aldehydes, nitriles and epoxides. *Organomet*. **2001**, *20*, 3169−3174.

(14) Brown, I. D. Chemical and steric constraints in inorganic solids. *Acta Crystallogr., Sect. B* **1992**, *48*, 553−572.

(15) Brown, I. D.; Altermatt, D. Bond-valence parameters obtained from a systematic analysis of the Inorganic Crystal Structure Database. *Acta Crystallogr., Sect. B* **1985**, *41*, 244−247.

(16) Palenik, G. J. (a) Bond valence sums in coordination chemistry using oxidation state independent R_O values. *Inorg. Chem*. **1997**, *36*, 122−122. (b) Bond valence sums in coordination chemistry using oxidation state independent R_O values. A simple calculation of the oxidation state of titanium in complexes containing Ti−N, Ti−O and Ti−Cl bonds. *Inorg. Chem*. **1997**, *36*, 3394−3397. (c) Bond valence sums in coordination chemistry using oxidation state independent R_O values. A simple method for calculating the oxidation state of manganese in complexes containing only Mn−O bonds. *Inorg. Chem*. **1997**, *36*, 4888−4890.

(17) Wood, R. M.; Palenik, G. J. Bond valence sums in coordination chemistry. A simple method for calculating the oxidation state of cobalt in complexes containing only Co−O bonds. *Inorg. Chem*. **1998**, *37*, 4149−4151.

(18) Kanowitz, S. M.; Palenik, G. J. Bond valence sums in coordination chemistry using oxidation state independent R_O values. A simple method for calculating the oxidation state of iron in Fe−O complexes. *Inorg. Chem*. **1998**, *37*, 2086−2088.

(19) O'Keefe, M.; Brese, N. E. Atom sizes and bond lengths in molecules and crystals. *J. Am. Chem. Soc*. **1991**, *113*, 3226−3229.

(20) Falvello, L. R. Jahn−Teller effects in solid-state coordination chemistry. *J. Chem. Soc., Dalton Trans*. **1997**, 4463−4475.

(21) Cirera, J.; Alemany, P.; Alvarez, S. Mapping the stereochemistry and symmetry of tetracoordinate transition metal complexes. *Chem. Eur. J.* **2004**, *10*, 190−207.

(22) Alvarez, S.; Llunell, M. Continuous symmetry measures of pentacoordinate molecules: Berry and non-Berry distortions of the trigonal bipyramid. *J. Chem. Soc., Dalton Trans*. **2000**, 3288−3303.

(23) Alvarez, S.; Avnir, D.; Llunell, M.; Pinsky, M. Continuous symmetry maps and shape classification. The case of six-coordinated metal compounds. *New J. Chem.* **2002**, *26*, 996−1009.

(24) Casanova, D.; Alemany, P.; Bofill, J. M.; Alvarez, S. Shape and symmetry of heptacoordinate transition-metal complexes: Structural trends. *Chem. Eur. J*. **2003**, *9*, 1281−1295.

(25) Raithby, P. R.; Shields, G. P.; Allen, F. H.; Motherwell, W. D. S. Structure correlation study of 4-coordinate copper(I) and (II) complexes. *Acta Crystallogr., Sect. B* **2000**, *56*, 444−454.

(26) Yao, J. W.; Copley, R. C. B.; Howard, J. A. K.; Allen, F. H.; Motherwell, W. D. S. General method for the description, visualization and comparison of metal coordination spheres: geometrical preferences, deformations and interconversion pathways. *Acta Crystallogr., Sect. B* **2001**, *57*, 251−260.

(27) Greenwood, N. N.; Earnshaw, A. In *Chemistry of the Elements*, 2nd ed.; Butterworth Heinemann: Oxford, 1997; pp 1164−1165.

(28) Coe, B. J.; Glenwright, S. J. Trans effects in octahedral transition metal complexes. *Coord. Chem. Rev.* **2000**, *203*, 5−80.
(29) Allen, F. H.; Mondal, R.; Pitchford, N. A.; Howard, J. A. K. Mapping the geometry of metal three-coordination using crystal structure data: Reaction pathway for ligand addition to linear Hg^{II} species. *Helv. Chim. Acta* **2003**, *86*, 1129−1139.
(30) Gütlich, P.; Garcia, Y.; Goodwin, H. A. Spin crossover phenomena in Fe(II) complexes. *Chem. Soc. Rev.* **2000**, *29*, 419−427.
(31) Sieber, R.; Decurtins, S.; Stoeckli-Evans, H.; Wilson, C.; Yufit, D.; Howard, J. A. K.; Capelli, S. C.; Hauser, A. A thermal spin transition in $[Co(bpy)_3][LiCr(ox)_3]$ ($ox=C_2O_4^{2-}$; bpy=2,2′-bipyridine). *Chem. Eur. J.* **2000**, *6*, 361−368.
(32) McAuliffe, C. A. In *Comprehensive Coordination Chemistry*; Wilkinson, G., Gillard, R. D., McCleverty, J. A., Eds.; Pergamon Press: Oxford, 1987; Vol. 2, Chapter 14, pp 1030−1041.
(33) Orpen, A. G.; Connelly, N. G. Structural systematics: Role of P−A σ^* orbitals in metal-phosphorus π-bonding in redox-related pairs of $M\text{-}PA_3$ complexes (A = R, Ar, OR.; R = Alkyl). *Organometallics* **1990**, *9*, 1206−1210.
(34) Anderson, K. M.; Orpen, A. G. On the relative magnitudes of *cis* and *trans* influences in metal complexes. *Chem. Commun.* **2001**, 2682−2683.

CI0500785